Soft body impact resistance of composite foam core sandwich panels with unidirectional corrugated and tubular reinforcements

Rade Vignjevic*, James Campbell*, Kevin Hughes*, Michał Orłowski, Serafina Garcea***, Philip Withers***, Julian Reed******

**Structural Integrity Theme*

Brunel University London, Kingston Lane, Uxbridge UB8 3PH

e-mail: v.rade@brunel.ac.uk

*** Centre for Mobility and Transport*

Coventry University, Priory Street, Coventry, UK, CV1 5FB

e-mail: orlowski.michal.adam@gmail.com

**** School of Materials*

The University of Manchester, Oxford Road, Manchester, UK, M13 9PL

e-mail: p.j.withers@manchester.ac.uk

e-mail: serafina.garcea@manchester.ac.uk

***** Rolls-Royce*

Registered office: 62 Buckingham Gate, London, UK, SW1E 6AT

e-mail: julian.reed@rolls-royce.com

Abstract

Bird strikes represent a major hazard in the lifecycle of composite aircraft components, due to the low impact resistance of composites. The research presented in this paper investigates soft body impact performance of composite sandwich panels with corrugated and tubular core reinforcements. This type of panel with augmented strength and stiffness in one direction is of high importance for specific aerospace applications. The panels were subjected to high velocity impact with soft gelatine projectile as used in bird strike tests. In addition, the experimental part included non-destructive inspections of the sandwich panel samples. Panel performance was also analysed with the non-linear transient analysis software LS-DYNA with finite element and SPH capability. The panel with corrugated reinforcement showed good impact resistance with damage restricted to the impacted face sheet, foam core and corrugated reinforcement. The panel with tubular reinforcement, of the same thickness, did not suffer any damage at the same impact velocity of 115 m/s, but was damaged at a higher impact velocity of 235 m/s. The numerical studies helped to understand the experimental data, enabling comparison of impact performance of the reinforced sandwich panels and a benchmark conventional sandwich panel. The proposed reinforced sandwich panels, with the desired augmented strength and stiffness in one direction, showed improved impact resistance in comparison to conventional sandwich panels and therefore have potential for application in aerospace structures where these properties are desirable.

Keywords: bird strike, composites, sandwich panel, tubular core reinforcement, corrugated core reinforcement, soft body impact, FEM, SPH, CT - computed tomography

1. Introduction

Composite sandwich structures are a class of composite materials combining stiff composite skins with a lightweight, low density core. This results in a structure with very high bending stiffness and low structural weight with widespread applications in aerospace and civil engineering. A range of core materials are typically used including honeycombs, balsa wood, open and closed cell non-metallic and metallic foams, e.g. polyurethane (PUR), polystyrene, polyvinylchloride (PVC), or metallic aluminium foam. For sandwich skins,

a range of options are available, with glass or carbon laminates being the most popular, through to metallic face sheets. Sandwich panels have been in use for more than a century, so there is a large body of publications covering all aspects of research related to them. The scope of the research presented required a review of literature related to experimental characterisation and modelling of impact response of sandwich panels.

Sandwich panels are routinely employed in aerospace, marine and offshore applications [1] due to their advantages in terms of bending stiffness, stability and weight reduction [2][3][4]. Despite the enhanced stability and stiffness properties of sandwich panels they often suffer from low impact resistance [5][6][7][8][9][10]. These studies showed that the impact resistance of composite sandwich structures is influenced by many different factors. The main factors which control the energy absorption, damage extent and damage modes are:

- Composite skin material (material type and layup),
- Face sheet thickness,
- Core material (density and crush properties),
- Core thickness,
- Impact characteristics (velocity, material, mass and shape of the impactor).

Horrigan, et al. [8] investigated the impact of soft and hard projectiles on a honeycomb core sandwich structure with glass fibre skin panels and observed shallow core crushing when impacted by a soft projectile. A hard projectile caused deeper core damage and more extensive skin damage. Charles & Guedra-Degeorges [10] demonstrated that the indentation depth is proportional to the impact energy up to a maximum limit depth. Mines, et al. [11] studied the perforation of sandwich panels with woven glass epoxy prepreg skins and honeycomb core and woven glass vinyl ester skins with a Coremat core. They found that energy absorption is controlled by core crushing and that the required perforation energy is a function of skin failure stress and the density dependent core strength at higher strain rates (strain rate sensitive) [12][13]. Furthermore, the authors observed that the core crushing dominated the energy absorption process, that initial skin delamination did not significantly influence through-thickness dynamic load bearing capacity.

Rhodes [14] showed that increasing the core crush strength improves the impact resistance of the sandwich structure. Raju, et. al. [4] investigated the impact response of honeycomb sandwich panels, finding that the peak impact force, was dependent on the core thickness, the size of the impactor and the type of face sheet and was not dependent on the boundary conditions (simply supported, fully fixed). By contrast, Flores-Johnson & Li [15] observed that the boundary conditions have a strong influence on the quasi-static indentation of foam core sandwich panels with carbon fibre face sheets. Further, they observed that the foam core density had significant influence on the energy absorption, damaged area and failure.

Hazizan & Cantwell [1] found that damage of PVC/PUR systems with brittle core materials was characterised by a shear fracture. For intermediate modulus systems samples failed due to composite skin buckling and for high modulus PVC/PUR systems failure was due to skin delamination of the impacted surface. This led to the conclusion that the dynamic response of foam-based sandwich structures is controlled by the core mechanical properties. Wang, et al. [16] examined the influence of face and core thickness on impact resistance of PUR foam-based sandwich panels with plain weave carbon fibre facings and made the following observations:

- Foam core thickness did not influence the impact response and damage extent,
- Increasing face thickness resulted in increased peak load and decreased contact duration,
- Ratio of absorbed energy to impact energy decreased with increasing face thickness,
- Face sheet thickness influenced damage diameter and indentation depth,
- Increase of the impact energy caused an increase of the absorbed/impact energy ratio, contact duration, the indentation depth and damage diameter.

Core reinforcement represents another approach for improvement of the impact resistance of sandwich structures. Torre & Kenny [17] concluded that the absorbed energy to deformation ratio could be doubled by incorporating a corrugated sheet into the sandwich core. Vaidya, et al. [18] investigated the high strain rate impact (164-327 m/s) response of sandwich panels with through-thickness reinforcements including honeycomb and foam core sandwich structures reinforced with steel, glass/epoxy and titanium Z-pins. The application of Z-pins showed considerable improvement in the impact resistance with a small increase in weight. Lascoup at. al. [19] investigated impact response of three-dimensional stitched sandwich composite

panels demonstrating benefits of the through thickness reinforcement. Subsequently, Vaidya, et al. [20] considered a novel composite design comprising E-glass fabric face sheets bonded together with vertical piles woven to the faces to form an integral 3D sandwich structure with PUR filled core. Low velocity impact tests showed no delamination under the impacts considered. Failure of the samples were dominated by core crushing. The PUR core increased the panel impact load carrying capacity by 250%.

Experimental characterisation of sandwich structures under impact loading combined with new imaging techniques, such as computed tomography, provide detailed information and allow for improved understanding of damage and failure. In spite of extensive research into their impact response it is still not fully understood [21][22]. Furthermore, experimental characterisation is time consuming and expensive [9][23][24][25]. In order to reduce the development & certification time and costs, experimentally validated numerical modelling is increasingly used to predict crash and impact response of sandwich structures. In addition, numerical modelling allows for optimisation of structural design including material properties. One of the key challenges in the modelling impact response of sandwich structures is complexity of their damage and failure mechanisms including damage of the composite skins [26]. Although the main damage mechanisms, e.g. matrix cracking, debonding and fibre failure may occur individually they often interact and occur simultaneously resulting in complex failure modes [27][28][29].

In the last few decades significant volume of research has been devoted to the development of simulation tools for modelling of sandwich structures. Here, we refer to few selected papers out of hundreds, related to modelling response of composite sandwich structures to impact loading [21][30][31][32][33][34].

A number of researchers, for instance [23][24][28][30][33][34][35][36][37][38] used shell elements to model the face sheets in order to reduce the computational time. Zhou et al. [34] studied the perforation resistance of sandwich panels with foam core using 2D elements for the face sheets. These elements could not accurately model the failure modes of the face sheets which are characterised by 3D stress states.

Feng et al. [32] used a progressive damage model to simulate the damage in sandwich composites with foam core subjected to impact loads where a 3D damage model was used to track the intra-laminar damages in face sheets and cohesive elements to model delamination. Morada at. al. [39] used modelling

to demonstrate advantages of sandwich composites made with a high-density core (ATH/epoxy: epoxy resin filled with alumina trihydrate particles) and non-Crimp Fabric (NCF) glass/epoxy face sheets. Besant et al. [40] used a model which takes into account large deflections, plastic deformation of the core and in-plane degradation of composite skins, to investigate damage behaviour of sandwich panels under low-velocity impact. Shi et al. [28] developed and validated a user-defined subroutine for a commercial code to model the damage due to in-plane cracking and delamination. Foo et al. [33] developed and experimentally validated a 3D model for damage prediction in composite sandwich structure. The model proposed by Schwab et al. [37] for modelling of impact on fabric reinforced laminated composites offers itself for modelling of face sheets where material nonlinearities due to damage were taken into account, including fibre breakage, intra-laminar and interlaminar cracking of matrix and interface failure. Menna et al. [36] proposed numerical models for glass fibre reinforced plastics sandwich panels with Nomex cores and investigated their strain-rate-dependent properties.

The presented work follows the potential of core reinforcement to improve impact resistance of composite sandwich panels identified by previous research. The reviewed approaches used in modelling behaviour of sandwich panels are fragmented, typically addressing some aspects of the physical behaviour well and failing to capture other equally important effects. It is evident that additional research is required especially on high velocity impact performance of reinforced sandwich structures, e.g. bird strike. This paper investigates, experimentally and numerically, performance of sandwich panels with corrugated and tubular reinforcements under soft body impacts representative of bird impact. The impact damage was mapped in 3D using X-ray tomography, pulsed thermography and in addition investigated through range of finite element/SPH based simulations to enable understanding of the response of the panels including damage.

The paper is organized as follows: Section 2, provides description of the experimental procedures used for material characterisation, the panel impact tests and the non-destructive techniques used. Further, in this section material parameters required for modelling are given. These parameters were obtained either from the manufacturers data sheets or determined by experimental characterisation. In Section 3 the impact tests results are presented and discussed. In Section 4 numerical modelling of the impact tests described in

Section 3 is presented and the results compared with the experimental data. Conclusions related to the outcome of this work are given in Section 5.

2. Experimental procedure

This section provides information about manufacturing of the samples and the experimental techniques used. In addition, it provides material parameters used in numerical modelling described in Section 4. This data is obtained either from the manufacturers data sheets or determined experimentally. To be precise, Vari-prepreg, wrapped carbon fibre tubes, the corrugated reinforcement and Permabond material parameters were taken as provided by the corresponding manufacturers. The foam material was manufactured and experimentally characterised in house. The manufacturers material data sources are referenced where appropriate.

2.1 Materials

Two different sandwich structures with through-thickness reinforcement were investigated. As illustrated in Figure 1, the first, a corrugated reinforced sandwich panel (CRSP), comprises a foam core reinforced with a corrugated carbon composite (CRSP) sheet bonded to the woven C-fibre face sheets, the second, a tubular reinforced sandwich panel (TRSP), incorporates foam filled (low density) C-fibre composite tubes bonded between woven carbon fibre face sheets. Table 1 summarise the configurations of the two panels.

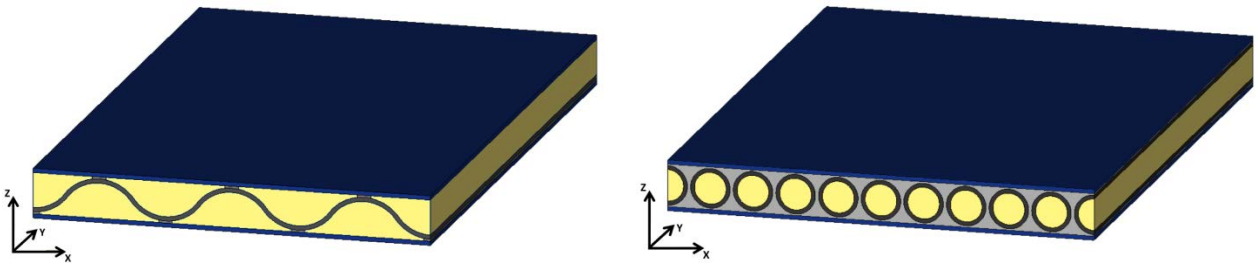

a) b)

Figure 1 Reinforced sandwich panels: a) Corrugated sandwich (CRSP) panel, b) Tubular sandwich (TRSP) panel.

The fibre reinforcements were all based on continuous Grafil 34-700 WD 12K Carbon high strength, PAN based fibres with filament diameter 7 μm, Tensile strength 4900 MPa, Tensile Modulus 250 GPa and Failure Strain 2%.

Table 1 The corrugated and tubular reinforced sandwich panel configurations

Geometry	CRSP	TRSP
Dimensions (mm)	100 x 150	
Face sheets	1 mm thick woven carbon fibre pre-pregs (EasyComposites Ltd., 2010)[42]	
Reinforcement	Four layers of ACG MTM46EL C fibre prepreg (UMECO, 2015)[41]	Roll Wrapped C Fibre Tubes (EasyComposites Ltd., 2010)[42]
Weight	90 grams	180 grams
Face sheet bonding	Permabond PT326 (EasyComposites Ltd., 2010)[42]	
Core	Two component polyurethane liquid foam (CFS Fibreglass) [43]	

According to the manufacturer's description [42] (Easycomposites, 2010), the carbon fibre sheets were produced in an autoclave from three layers of carbon fibre Twill pre-preg. The exact layup schedule and ply orientations of the material are shown in Table 2 and the material properties are shown in Table 3.

The tubular sandwich panel was reinforced with 10 mm Roll Wrapped Carbon Fibre Tubes supplied by Easy Composites. The tubes were manufactured from high modulus Toray T700 unidirectional carbon fibre prepreg and E-Glass UD (80/20). The tube fibres were oriented in 0^o and 90^o directions which ensures superior mechanical properties in comparison to the pultruded tubes which have fibres only in one direction. The layup of a single tube is given in Table 4 and its material properties are given in Table 5.

The corrugated panels were manufactured from ACG MTM46EL prepreg, a medium temperature, toughened epoxy system intended for aerospace applications. The mechanical properties of MTM46EL are given in Table 6. The mould for the corrugated shape was manufactured based on a PVC corrugated sheet.

Table 2 Layup schedule for Easycomposites prepreg carbon fibre sheet [42].

Schedule	Ply orientation
204g 2/2 Twill 3k Prepreg Carbon Fibre	0^o, 90^o
430g 2/2 Twill 12k Prepreg Carbon Fibre	0^o, 90^o
204g 2/2 Twill 3k Prepreg Carbon Fibre	0^o, 90^o

Table 3 Vari-prepreg material properties [42]

Property	Test method	Value
Flexural strength	EN2562	850 MPa
Flexural modulus	EN2562	59000 MPa
Tensile strength	ISO 527	650 MPa
Tensile modulus	ISO 527	59000 MPa
ILSS - Short Beam Shear	EN2563	65 MPa

Table 4 Layup schedule for the carbon fibre roll wrapped tubes [42].

Schedule	Ply orientation
300 g/m^2 Toray T700	0^o
300 g/m^2 E- UD	90^o
300 g/m^2 Toray T700	0^o
300 g/m^2 E- UD	90^o
300 g/m^2 Toray T700	0^o

Table 5 Carbon fibre roll wrapped tube material properties [42].

Property	Value
Density	1.6 g/cm^3
Young's Modulus 0^o	70000 MPa
Young's Modulus 90^o	70000 MPa
Ultimate tensile strength 0^o	600 MPa
Ultimate compressive strength 0^o	570 MPa
Ultimate tensile strength 90^o	600 MPa
Ultimate compressive strength 90^o	570 MPa

The components of these panels were bonded together with, Permabond PT326, polyurethane adhesive suitable for bonding a wide variety of materials including plastics, composites and metals. The material properties of the cured adhesive are given in Table 7.

A two-component polyurethane low-density foam system supplied by CFS Fibreglass Supplies was chosen for the core material. The foam is manufactured by mixing two liquid components, Tripor 227 Components A and B at a ratio 1 to 1.13 by weight or 1:1 by volume. Its liquid form and uniform expansion make this foam suitable for filling of cavities. The mixture was injected into the cavities of the corrugation and tube reinforced sandwich panels. Following expansion and solidification surplus foam was removed. The same procedure was used to inject the foam into specially designed containers to produce samples required for mechanical characterisation. This process is described in detail in [63]. The quality of filling was checked by thermal imaging as described in Section 2.3.1.

Table 6 MTM 46 EL material properties [41].

Property	Test method	Value
Tensile modulus	D3039	55800 MPa
Compressive modulus	D3410	53300 MPa

Transverse tensile modulus	D3039	56400 MPa
Transverse compressive modulus	D3410	51900 MPa
Tensile strength	D3039	497 MPa
Compressive strength	D3410	698 MPa
Transverse tensile strength	D3039	513 MPa
Transverse compressive strength	D3410	706 MPa
Tensile strain to failure	D3039	0.9 %
Compressive strain to failure	D3410	1.3 %
Transverse tensile strain to failure	D3039	0.92 %
Transverse compressive strain to failure	D3410	1.37 %
In-plane shear modulus	D3518	3510 MPa
In-plane shear strength	D3518	113.4 MPa
Min. tensile Poisson's ratio	D3039	0.04
Max. compressive Poisson's ratio	D3410	0.04
Min. tensile Poisson's ratio	D3039	0.05
Max. compressive Poisson's ratio	D3410	0.05
ILSS (WARP)	D2344	71.8 MPa
ILSS - Short Beam Shear	EN2563	65 MPa

1

2 Table 7 Permabond PT326 material mechanical properties [42]

Property	Test method	Value
Shear strength	ISO 4587	9 - 11 MPa
Tensile strength	ISO 37	16 - 25 MPa
Elongation at failure	ISO 37	< 15% MPa
Hardness	ISO 868	65 - 75 Shore D
Coefficient of thermal expansion	ASTM D-696	85 x 10^{-6} K^{-1}
Peel strength		150-170 N/25 mm

The core material was modelled with a crushable foam material model available in LS-DYNA. Determination of the input parameters for the crushable foam material model require experimental data in the form of stress vs. volumetric strain curve under the compressive loading followed by unloading. The mean curve used for determination of the input parameters was obtained by averaging data from six tests. The core material is characterised by very small Poisson's ratio which allowed for simple calculation of volumetric strain based on the initial sample size and recorded test machine head displacement. The quasi-static compression tests were conducted according to the ASTM C365/C365M-05 standard, which specifies the test methods for compressive properties of sandwich cores. The sample dimensions were 50 mm x 50 mm x 30 mm. The polyurethane foam density ρ = 60.78 kg/m^3 was determined by averaging the density of the manufactured foam samples.

Based on the mean stress-strain curve (see Figure 2), the plateau stress was defined as σ_p = 0.39 MPa and the maximum stress for the maximum measured volumetric displacement of Y_{max}= 0.85 was σ_{max}= 1.9 MPa.

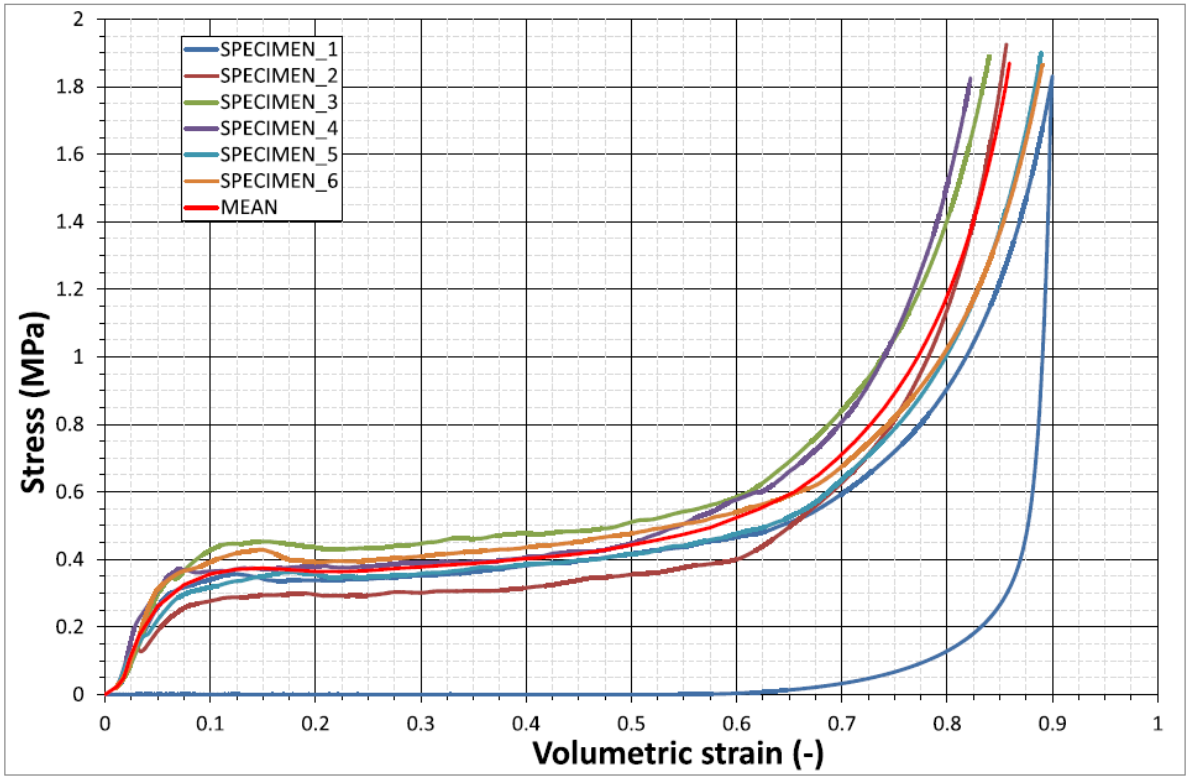

Figure 2. Stress volumetric strain curves from the six compression tests and the mean value curve used to generate input data for the foam model

At present, artificial gelatine birds are used in the process of aircraft certification as a substitute for the real birds. In spite of the effort to standardise the artificial birds, for instance see Hamershock at. al. [44], there is no uniquely accepted specification of artificial birds. The birds used in this investigation were manufactured following the procedure proposed by Lavoie et. al. [45] due to the realistic representation of the real bird demonstrated by Lavoie et. al. [46], as well as the relatively simple manufacturing process. Unlike the procedures used by Wilbeck [47], Lavoie's procedure does not require the use of rotating moulds during the gelatine solidification process. The manufactured birds had density of 0.97 g/cm^3 with homogeneous isotropic texture and sufficient stiffness to be launched from a gas gun.

2.2 Soft body impact tests

A 32 mm diameter single stage nitrogen driven gas gun [48], shown in Figure 4, with the capability to launch the projectiles at velocities up to 340 m s^{-1} was used to perform the impact tests. The cylindrical gelatine projectiles, shown in Figure 3, have diameter of 25 mm and the length of 50 mm, i.e. the length to diameter ratio of 2:1, as recommended by Budgey [49]. As already stated, the gelatine projectiles were manufactured using the approach described in [45][46]. The sabot stripper located close to the muzzle of the barrel successfully stopped polycarbonate sabots and enabled accurate projectile velocity measurement and repeatability of tests.

Figure 3 Gelatine projectiles and sabots prepared for the testing

According to Federal Aviation Administration report [50], 35% bird strikes occur during take-off and (61%) during landing. Therefore, as the worst-case scenario the impact velocity of 115 m/s, higher than take-off speed for most operating aircraft, was chosen for this investigation.

The projectiles were designed to allow characterisation of the reinforced sandwich panels (including damage and failure) under soft body impact resembling bird strike. The similarity is ensured through the similar shock wave strength, dynamic pressure magnitude and specific momentum.

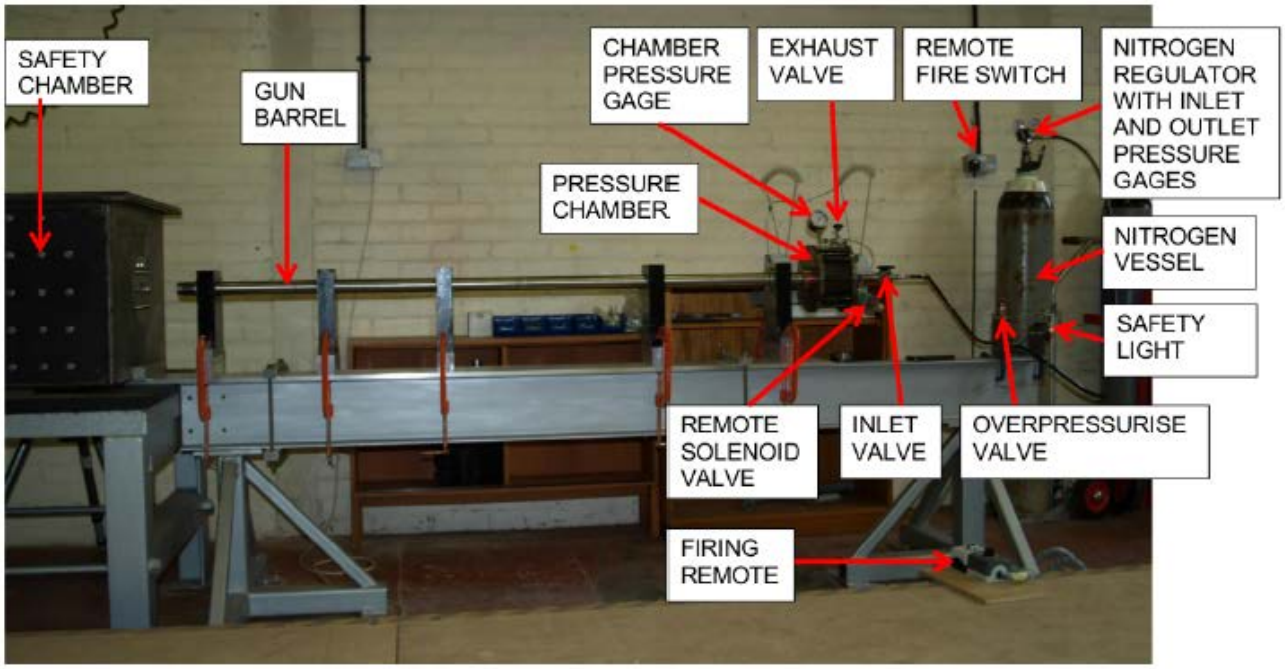

Figure 4 Single stage gas gun test facility

The projectile velocity was measured with an optical velocity measurement system mounted on the barrel muzzle. In addition, the impact sequence was recorded with a high-speed camera with a sampling rate of 10,000 frames per second.

The sample panels were clamped at the top and bottom to the steel frame as shown in Figure 5. The panel centres were aligned with the longitudinal axis of the barrel. However, due to the complex process of the projectile release (sabot stripping), the impact location varied ±5 mm from the barrel aiming point. The unconstrained span of the panels between the supports was 110 mm.

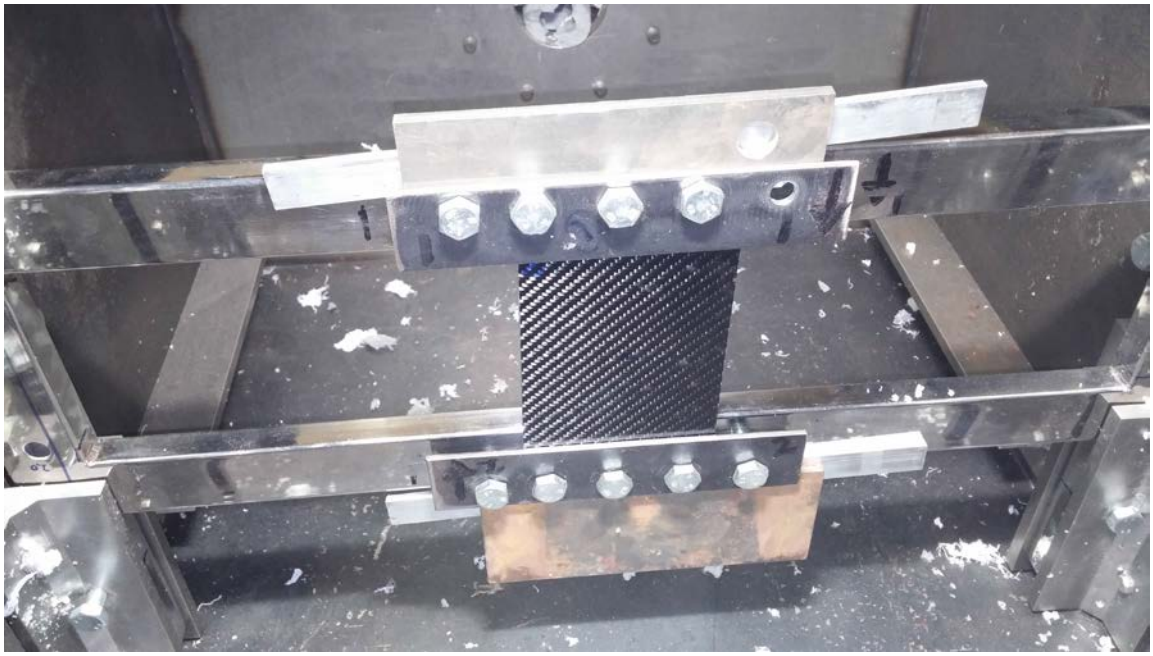

Figure 5 The boundary conditions used in the experiments

2.3 Damage inspections techniques

2.3.1 Pulsed thermography

Due to its ability to relatively quickly scan large sample and our limited access to X-ray imaging, pulsed thermography (PT), Shepard [51][52], was used for non-destructive assessment of manufactured samples for possible imperfections. The inspections were performed with the ThermoScope system (for details see [53]) capable of generating millisecond long light pulses with energy of approximately 25 kJ. The thermal responses of the samples were recorded with a long wavelength infrared camera XENICS GOBI 384, having a resolution of 384 x 512 pixels and sensitivity of 50 mK. In addition to the infrared images, temperature histories were also recorded at specific locations (points labelled with coloured markers in Figure 7 and Figure 9) to quantitatively assess the samples. The samples use in the experiments did not have any significant imperfections above the level typical for the manufacturing process used.

2.3.2 X-ray computed tomography

X-ray computed tomography (CT) was conducted at the Henry Moseley X-ray Imaging Facility at the University of Manchester using a Nikon 225/320 kV system. CT scanning of composite panels is not straightforward for two main reasons: (i) typical panel dimensions do not allow high resolution scanning of

the whole panel; (ii) the beam transmission during the sample rotation (360°) is not constant due to the significant difference in path length through the attenuating composite material when illuminated normal to, and parallel to, the panel. The latter effect was minimised by stacking together 3 panels to form a 'cube' to achieve a similar x-ray path length trough the material for all the projections.

An accelerating voltage of 70 kV, current of 50 µA and the voxel size equivalent to 60 µm were used in the scanning. This coupled with a detector of 2000x2000 16-bit pixels, resulted in an overall field of view of 120 mm (with) x 180 mm (height). For each scan 3142 projections were collected over 360°.

3. Results and discussion

3.1 Impact test results

A sequence of images for a CRSP test at a measured impact velocity of 116 m/s is shown in Figure 6, which shows the well-preserved shape of the projectile at the time of impact. During impact the projectile behaves as a fluid, imparting pressure loading to the panel. The results for all six tests are summarised in Table 8. The measured impact velocities show a small degree of scatter (average error of 0.5%), which illustrates the repeatability of each test.

Visual inspection of both type of samples revealed that two out of three corrugated samples had visible damage on the impacted surface. Erosion damage was limited to the impact location. By contrast, none of the tubular samples suffered any detectable damage. Since no damage was observed in tubular samples for the impact tests at V_i=115 m/s, additional tests were performed on the same samples at impact velocity of approximately V_i=245 m/s.

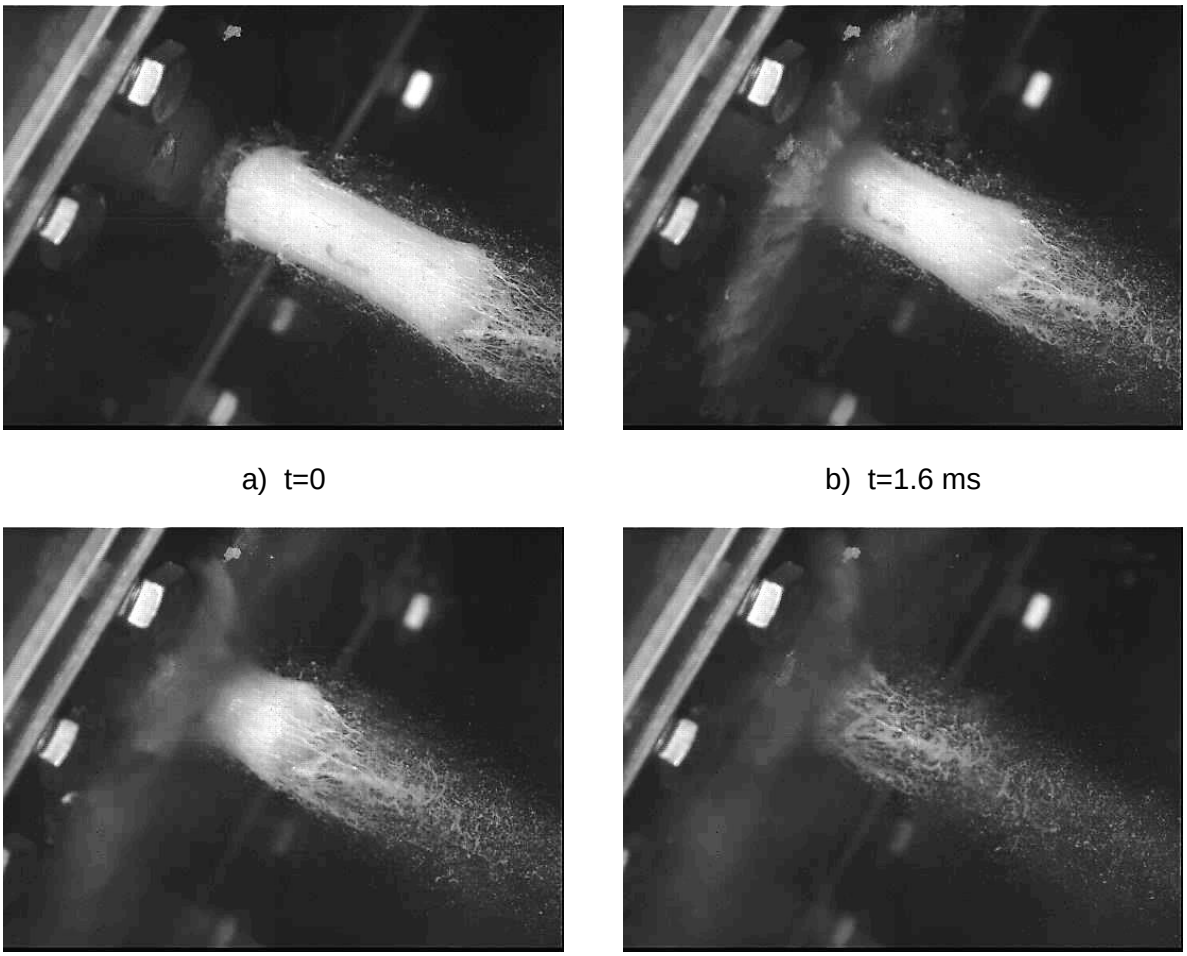

a) t=0 b) t=1.6 ms

c) t=3.2 ms d) t=4.8 ms

Figure 6 Impact sequence for CRSP 1 (V_i=116 m/s) at time intervals of 0.16 ms.

Table 8 Summary of the impact tests

Sample	Impacted side	Pressure (bar)	Impact velocity (m/s)	Impact energy (J)	Front Surface damage	Internal damage	Rear surface damage
CRSP_1	Bottom*	6	116.4	174	Yes	Yes	No
CRSP_2	Bottom*	6	114.6	167	Yes	Yes	No
CRSP_3	Bottom*	6	116.3	165	No	Yes	No
TRSP_1	N/A	6	116.0	166	No	No	No
TRSP_2	N/A	6	116.5	167	No	No	No
TRSP_3	N/A	6	119.7	175	No	No	No
TRSP_1	N/A	38	235.7	714	Yes	Yes	Yes
TRSP_2	N/A	40	254.1	783	Yes	Yes	Yes
TRSP_3	N/A	38	242.3	755	Yes	Yes	Yes

*As shown in Figure 1

3.2 Post impact sample assessments

3.2.1 Corrugated sandwich panel, impact velocity V = 116 m/s

In all CRSP tests centre of the panel was targeted which corresponds to the corrugation number four in Figure 7 and Figure 8. In those tests there was no visible damage, however significant amount of damage was detected by CT as discussed below.

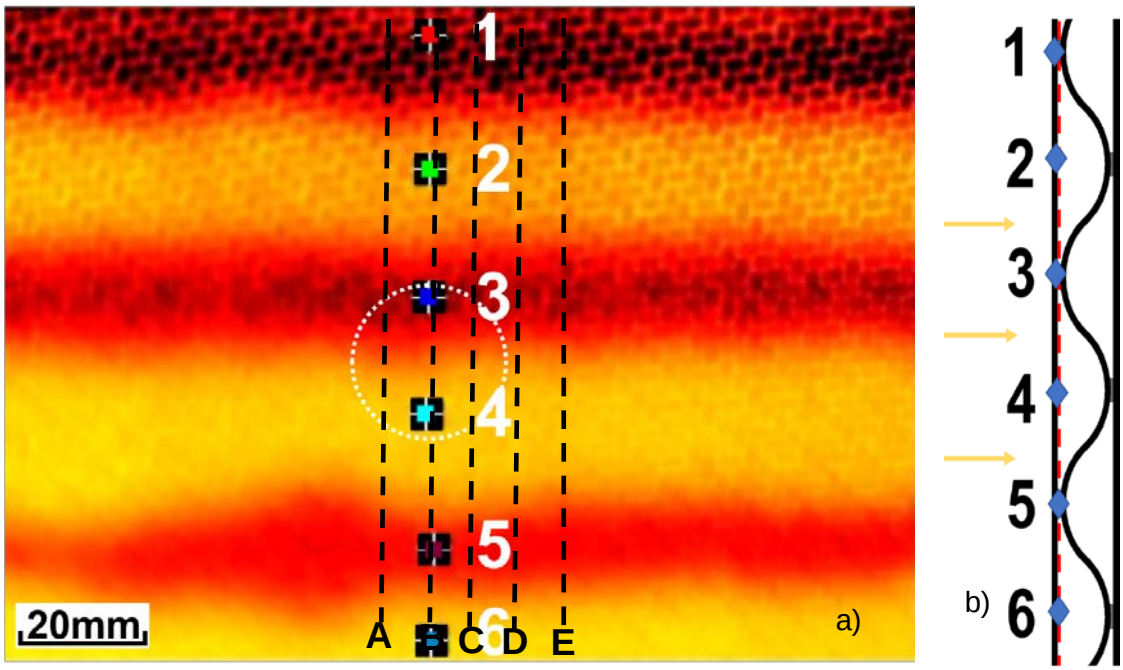

Figure 7. a) Post manufacturing thermography inspection of CRSP_1 measurement time t=0.56 s with no significant manufacturing imperfections in the sample; A, B, C, D & E cross sections for which post impact CT scans are given in Figure 8, b) sample cross section (arrows indicate heat flux direction)

Slices from the post-impact CT imaging for CRSP_1 which correspond to the cross sections (A, B, C, D & E) defined in Figure 7 are shown in Figure 8. In addition to some mid-plane porosity, introduced by manufacturing and marked Manu (not detected by PT), impact induced damage is clearly visible. It is evident that the impact has caused cracking and delamination (marked by the label Delam) within the impacted face sheet. Further, cracking between the second and fourth corrugation (marked Fract) and delamination of the corrugated reinforcement was also observed. In few locations the corrugation impact damage was initiated from pre-existing manufacturing defects. In Figure 8 b) and d) the same damage propagating along the corrugations can be seen. Localised erosion damage of the impacted face sheet combined with the delaminated is visible above the fifth corrugation wave in cross sections B to D. Cross section A and E show fracture of the impacted face sheet combined with delamination damage above the fourth corrugation.

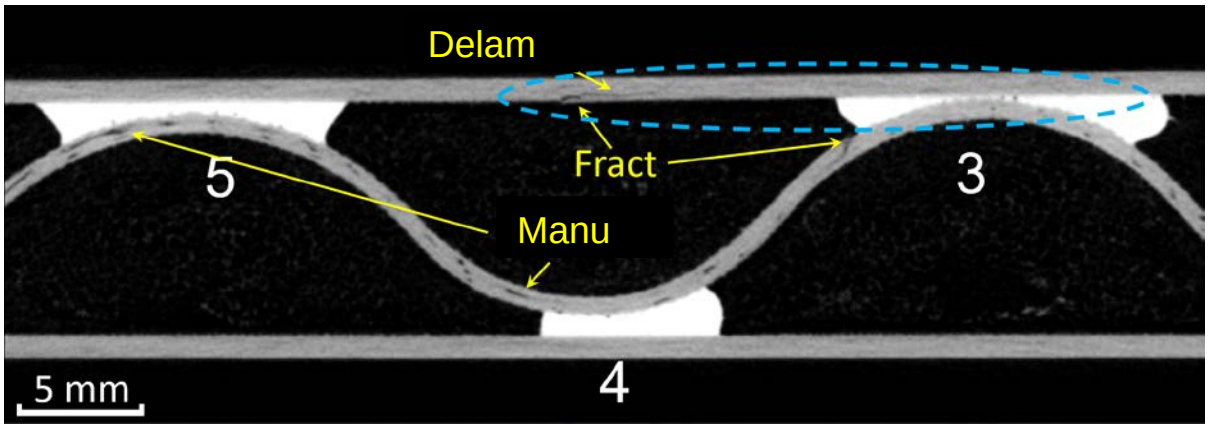
Delam
Fract
5
3
Manu
5 mm
4

a)

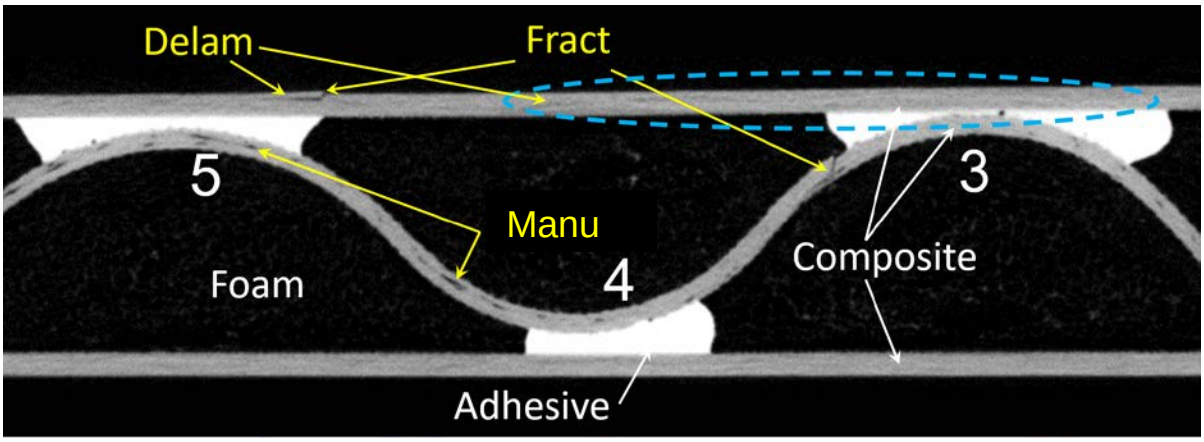
Delam
Fract
5
3
Manu
Foam
4
Composite
Adhesive

b)

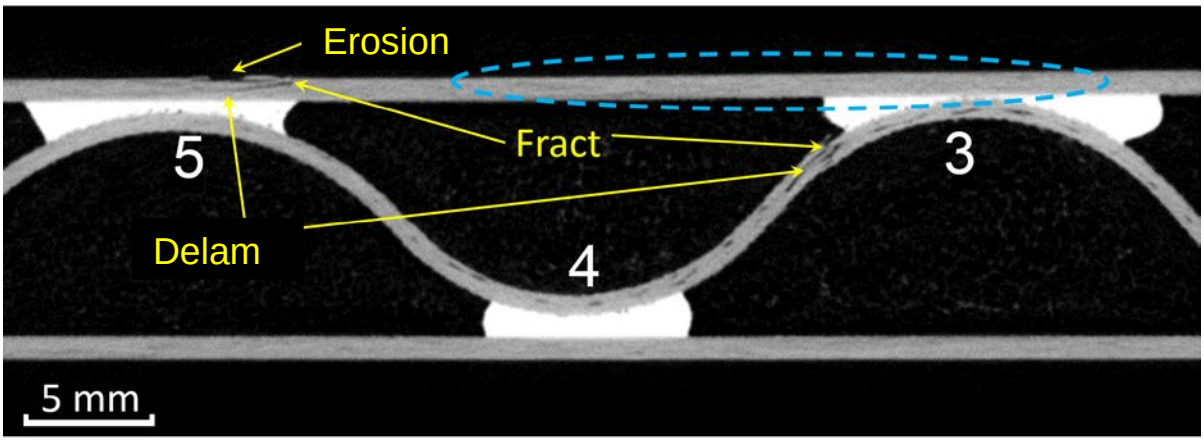
Erosion
Fract
5
3
Delam
4
5 mm

c)

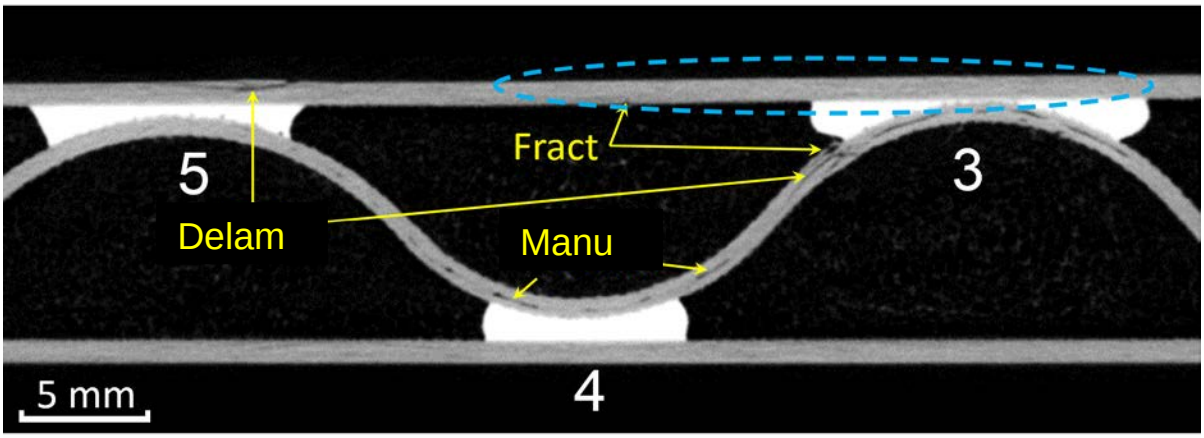

d)

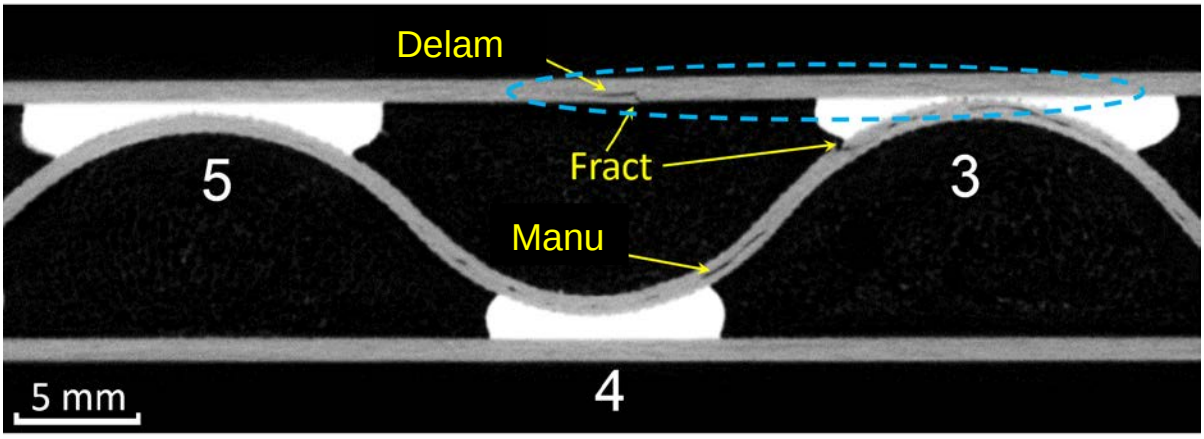

e)

Figure 8. Post impact CT scans for test CRSP_1. The cross sections A, B, C, D & E are as outlined in Figure 7 with the extent of damage A) 63 mm, B) 69 mm, C) 76 mm, D) 82 mm, E) 88 mm. The barrel targeted corrugation number 4, real impact location is marked with the blue ellipsoid.

Equivalent images for samples CRSP_2 and CRSP_3 are not shown due to very similar damage pattern.

3.2.2 Tubular sandwich panel, impact velocity 235 m/s

In all TRSP tests centre of the panel was targeted which corresponds to the tube number four in Figure 10 and Figure 11. The NDT inspection of TRSP_1 after the impact test performed at 116 m/s showed no evidence of damage. Based on this the decision was made to double the impact velocity in order to ensure that the panels would be damaged and allow for assessment of type and extent of damage. Due to limitation in repeatability of the projectile velocities the average impact velocity in the tests was 235 m/s instead of

instead 232 m/s. One of the images from PT inspection of the manufactured TRSP_1 indicating no presence of any significant manufacturing imperfections is shown in Figure 9.

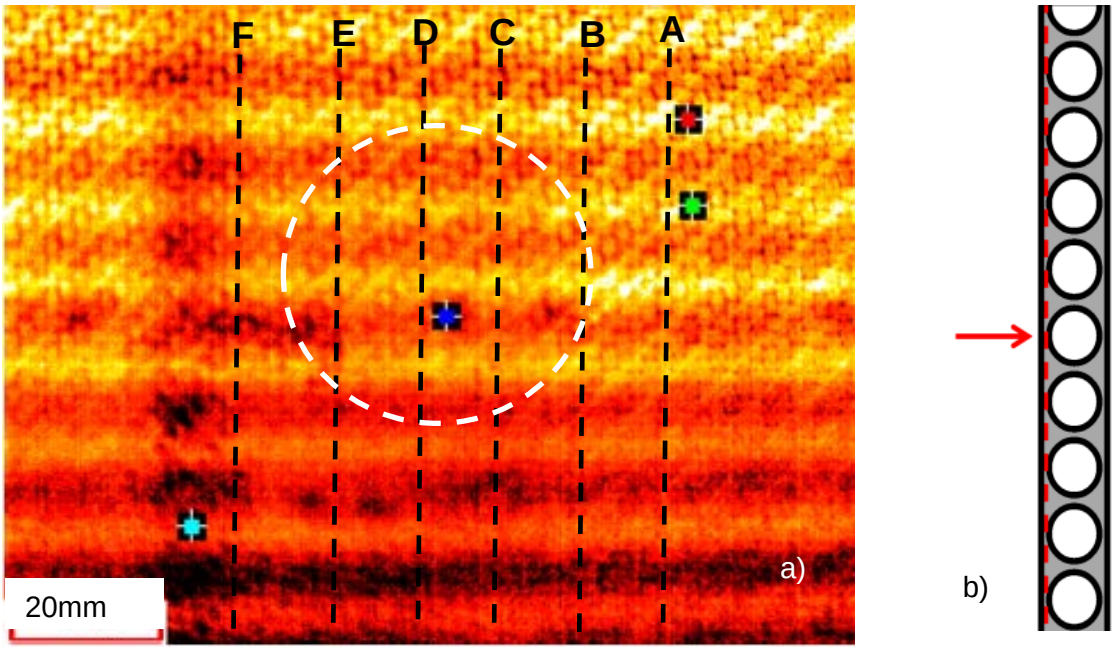

Figure 9. a) Post manufacturing thermography image of the TRSP_1 impact side at t=0.4 s with no significant manufacturing imperfections in the sample; A, B, C, D, E & F cross sections for which CT scans are given in Figure 10, b) the TRSP cross section with the heath flux vector indicated in the diagram

Virtual slices selected from the post impact CT imaging of TRSP_1 are shown in Figure 10. The de-bonding of the back-face sheet is clearly visible in Figure 10 a) marked as Debond. Further, two cracks are visible in the adhesive bond between the 5th and 6th tube (marked Adh Crack). The cross sections B to E in Figure 10 also show de-bonding between the 5th tube and the surrounding adhesive, as well as between the top face sheet and the adhesive. In addition to the adhesive damage, the CT images (Figure 10 B - E) show delamination and fibre rupture damage in the tubes number 4th, 5th and 6th. Damage extent for the considered cross sections was as follows: A) 63 mm, B) 71 mm, C) 76 mm, D) 82 mm, E) 90 mm, F) 98 mm (Figure 10 A-F).

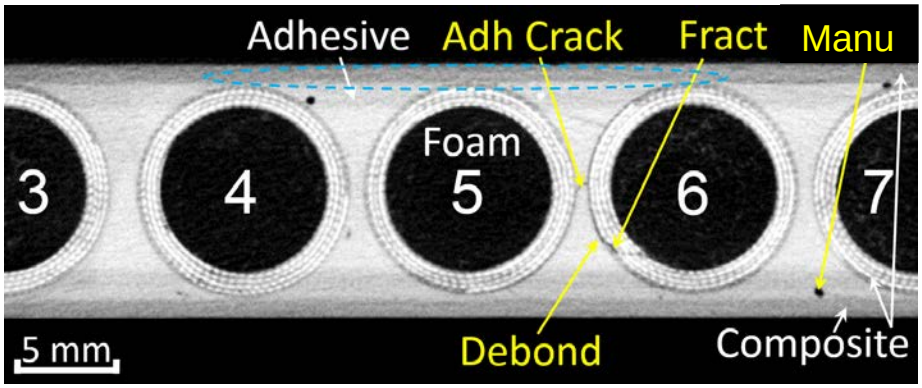
Adhesive
Adh Crack
Fract
Manu
Foam
3
4
5
6
7
5 mm
Debond
Composite

A)

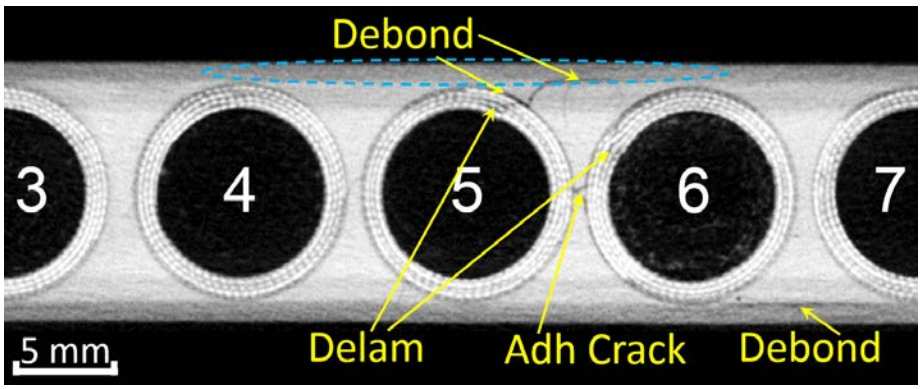
Debond
3
4
5
6
7
5 mm
Delam
Adh Crack
Debond

B)

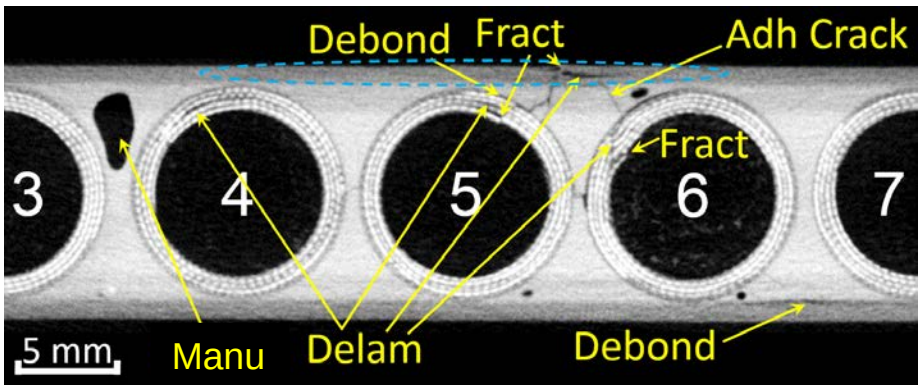
Debond
Fract
Adh Crack
Fract
3
4
5
6
7
5 mm
Manu
Delam
Debond

C)

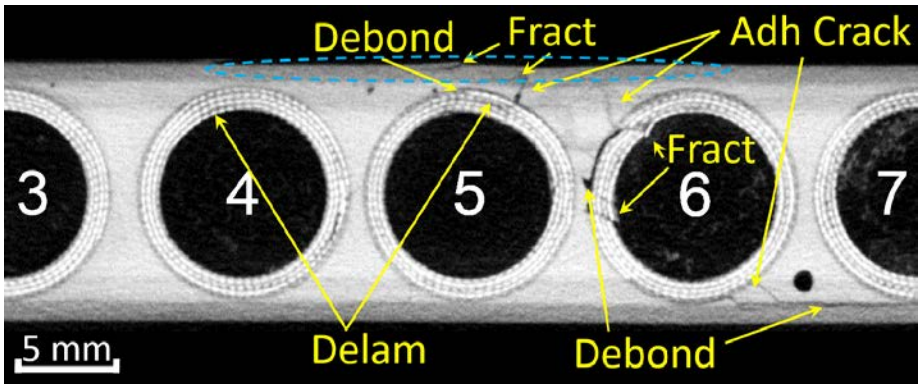
Debond
Fract
Adh Crack
Fract
3
4
5
6
7
5 mm
Delam
Debond

D)

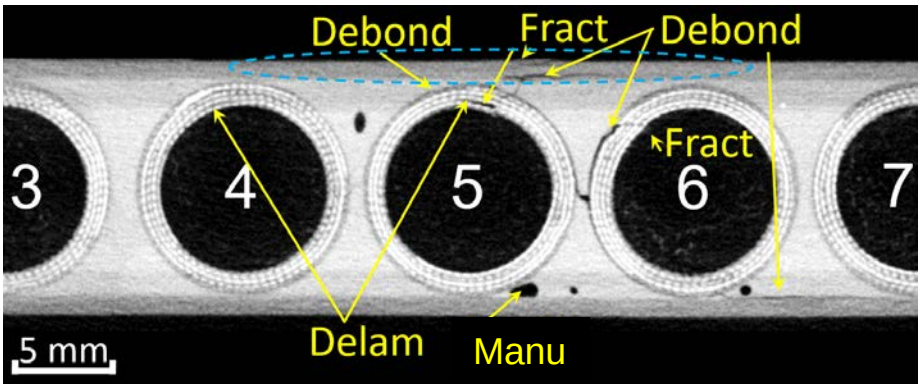

E)

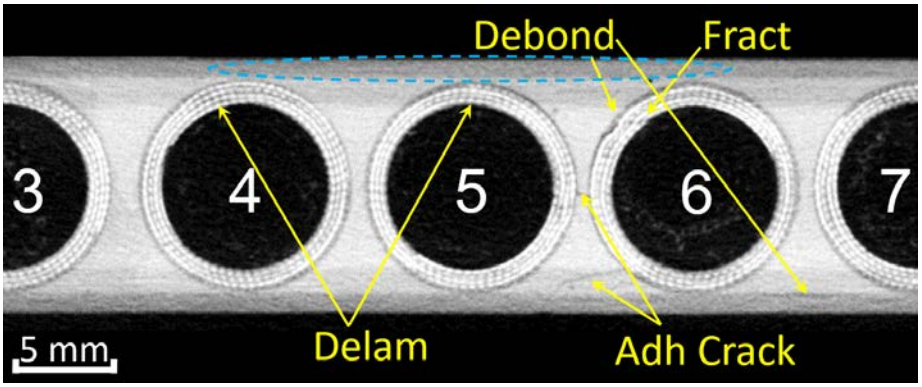

F)

Figure 10. Post Impact CT scans for TRSP_1; impact velocity V_{dt} = 235 m/s; Cross sections A, B, C, D, E & F are as outlined in Figure 9Figure **9** with the extent of damage A) 63 mm, B) 71 mm, C) 76 mm, D) 82 mm, E) 90 mm, F) 98 mm

The most severe adhesive damage occurred in the vicinity of the impact location (marked by the ellipsoid in Figure 10 – between 5th and 6th tube) and propagated from the impact point along the tubes. The extent of this damage was approximately 120 mm along the tube's direction (see Figure 11). The CT imaging provided a very clear insight into the types and the extent of damage in the samples.

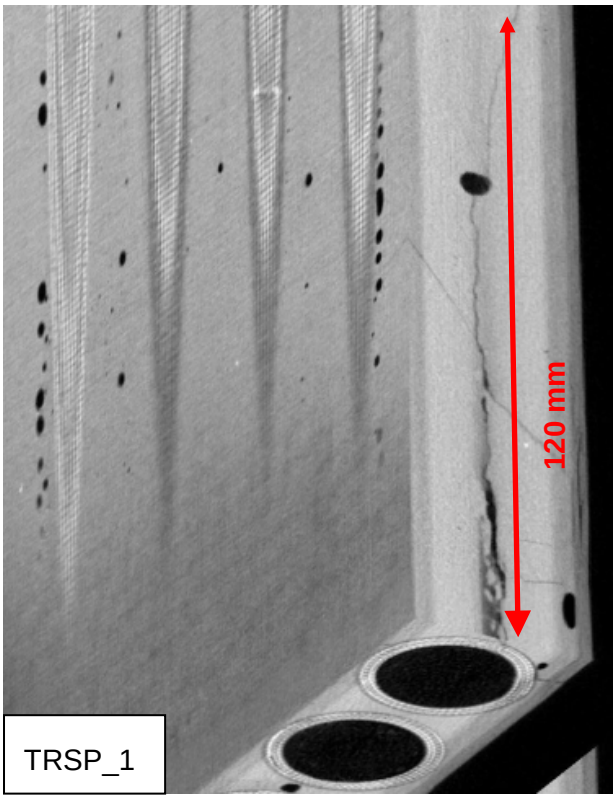

Figure 11 Damage at the interface between the tubes number 5 and 6, the tube numbering defined in Figure 10

4. Numerical analysis

In order to interpret the experimentally observed damage patterns numerical modelling was undertaken with a transient nonlinear FE solver (version R10.1.0 MPP was used for all results shown).

4.1 Projectile model

Even though the projectile used for the experiment was initially cylindrical, during the release from the sabot the flat front and rear projectile surfaces became rounded (see Figure 3 a). Therefore, the projectile was modelled as a hemispherical-ended cylinder in order to match the experiments. The projectile was discretised using 21,000 SPH particles with a 1 mm inter-particle distance, initial smoothing length h=1.2 mm (1.2 inter-particle distance) and uniform distribution of the particles. An ELASTIC_PLASTIC_HYDRODYNAMIC material model with a Linear Polynomial equation of state was used to model behaviour of the projectile; an approach commonly found in the literature Vignjevic, et al. [54], McCarthy, et al. [55] and Jenq, et al. [56]. The diameter d_b = 25 mm corresponds to the diameter of the

projectile used for the projectile impact tests. The length to diameter ratio of the projectile was equal l/d=2. The projectile material properties are given in Table 9.

Table 9 Projectile material properties for elastic-plastic-hydrodynamic material model:

Parameter	Value	[unit]
Density ρ	970	kg/m^3
Shear modulus - G	2.07	GPa
Yield stress - σ_y	0.02	MPa
Plastic hardening modulus - E_H	0.001	MPa
C_0	0.0	MPa
C_1	2323	MPa
C_2	5026	MPa
C_3	15180	MPa

Verification of the projectile model was performed in two stages. The first stage considered impact against rigid targets, with the pressure history at the point of impact compared against analytical values for the initial and steady state pressures used by Wilbeck [47] in his analysis of bird strike. The second stage considered impact on an aluminium sheet and compared the final shape of the panel against experimental data. In the both comparisons good agreements were achieved.

The initial set of impact simulations on the composite panel model revealed that this projectile model was too coarse. The contact algorithm used for the projectile-panel interaction was a node to surface algorithm, where an SPH particle interacts with a single contact segment. The 1 mm projectile inter-particle distance was greater than the minimum element edge length (0.58 mm) resulting in an uneven distribution of the contact force over the plate surface. The projectile model was refined to use an inter-particle distance of 0.25 mm to ensure that multiple SPH particles are interacting with each contact segment, providing a more even and representative impact load on the panel. The resulting projectile model contained 1,309,984 SPH particles, and to manage the computational cost the *DEFINE_BOX_SPH option was used so that only particles in the impact location were included in the neighbour search algorithm.

4.2 Modelling of the reinforced sandwich panels

Following the validation of the projectile model, the reinforced sandwich panels were modelled. Figure 12 a) and b) show the cross sections and Figure 13 a) and b) the complete discretised panels of the corrugated and tubular panel respectively. Element size in the cross-section was chosen following a convergence analysis where three different mesh densities were considered.

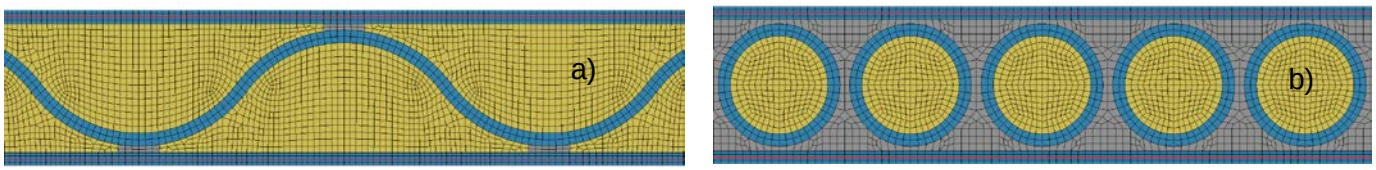

Figure 12 Cross sections of the discretised composite sandwich panels where blue elements represent composite material, grey the adhesive and yellow the polyurethane foam. a) CRSP, b) TRSP.

In CRSP and TRSP models the impacted and back face sheet panels, 1 mm thick, were modelled with four elements (with single point of integration) through the thickness in order to capture bending effects. The in-plane (i.e. X-Y plane, see Figure 15) element sizes for CRSP and TRSP were 0.525 mm x 0.900 mm and 0.589 mm x 0.840 mm respectively, in the vicinity of the impact location. Further away from the impact location the element size was increased in order to reduce computation time. The corrugated panel and the tubes were modelled using two fully integrated elements through the thickness in order to capture bending effects and to prevent numerical instabilities.

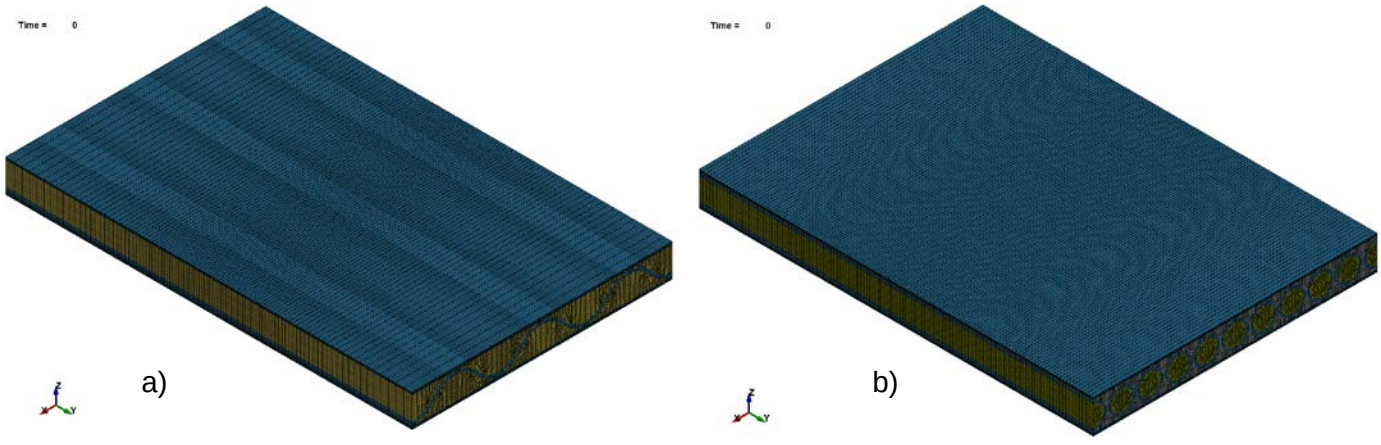

Figure 13: Isometric view of composite sandwich panel models with blue elements representing composite material, grey the adhesive and yellow the polyurethane foam. a) CRSP, b) TRSP.

1 The constitutive models used to model different parts of the sandwich panels is shown in Table 10 with the
2 specific material parameters given in Table 11.

3 Table 10 Material models used for modelling of composite sandwich panels

Material	Material model	Description of material model
Composite	MAT_59 - MAT_COMPOSITE_ FAILURE_SOLID_MODEL	Allows composite failure in three directions. Material failure is governed by failure criteria [57] which when satisfied sets stresses and material stiffness to zero. Complete failure of the material is represented by material erosion, which occurs when the stresses in all three directions σ_x, σ_y and σ_z are equal to zero [58]. Constant stress solid elements with a single integration point (element type 1) were used. MAT_59 [62] allows for definition of up to 8 additional history variables which enable for distinction of failure modes within the material (based on corresponding failure criterion).
Polyurethane adhesive	MAT_13 - MAT_ISOTROPIC_ ELASTIC_FAILURE	Non-iterative plastic material model with a simple plastic strain failure criterion [33]. Allows for elastic and shear behaviour of the adhesive. The failure of the material is based on the plastic failure strain, with optional erosion of failed elements activated in this case.
Polyurethane foam	MAT_154 - MAT_DESHPANDE_ FLECK_FOAM	An isotropic, continuum based material model for crushable foams [59], based on the Deshpande and Fleck foam model [60]. It allows for shear and tensile failure of the foam material resulting in erosion of failed elements. Failure is governed by a strain-based fracture criteria implemented into LS-DYNA by Reyes, et al. [61]. The decision to use this material model for the polyurethane foam was based on a range of single element test and simulation of indentation experiments

4

Table 11 Material properties for panel parts.

Composite part material properties (*MAT_COMPOSITE_FAILURE)				
Parameter	**Value**		**Parameter**	**Value**
Density	1600 kg/m^3		Shear strength S_{BA}	150 MPa
E_A	59.0 GPa		Shear strength S_{BA}	150 MPa
E_B	59.0 GPa		Shear strength S_{BA}	150 MPa
E_C	18.6 GPa		Compressive strength XXC	850 MPa
ν_{BA}	0.04		Compressive strength YYC	850 MPa
ν_{CA}	0.007		Compressive strength ZZC	483 MPa
ν_{CB}	0.007		Tensile strength XXT	650 MPa
G_{AB}	3.1 GPa		Tensile strength XXT	650 MPa
G_{BC}	1.17 GPa		Tensile strength XXT	60 MPa
G_{CA}	1.5 GPa			
Adhesive part material properties (*MAT _ISOTROPIC_ELASTIC_FAILURE)				
Density	1200 kg/m^3		Hardening modulus	8.5 GPa
Shear modulus	6.0 GPa		Bulk modulus	24.0 GPa
Yield stress	125 MPa		Plastic strain at failure	0.65
Foam part properties (*MAT_DESHPENDE_FLECK_FOAM)				
Density	60 kg/m^3		Densification strain	6.5
Elastic modulus	192 MPa		Alpha 2	1,000,000
Poisson's ratio	0.3		Beta	8.34
Alpha	1.0		Sigp	3.44 MPa
Gamma	1.0		Failure volumetric strain	0.2

In the experiment the panel ends are clamped between two steel plates, with the clamping force generated by a set of bolts visible in Figure 5. These steel plates are represented in the model as steel sections, shown in Figure 14. Springs with a pre-tension force are used to represent the bolts.

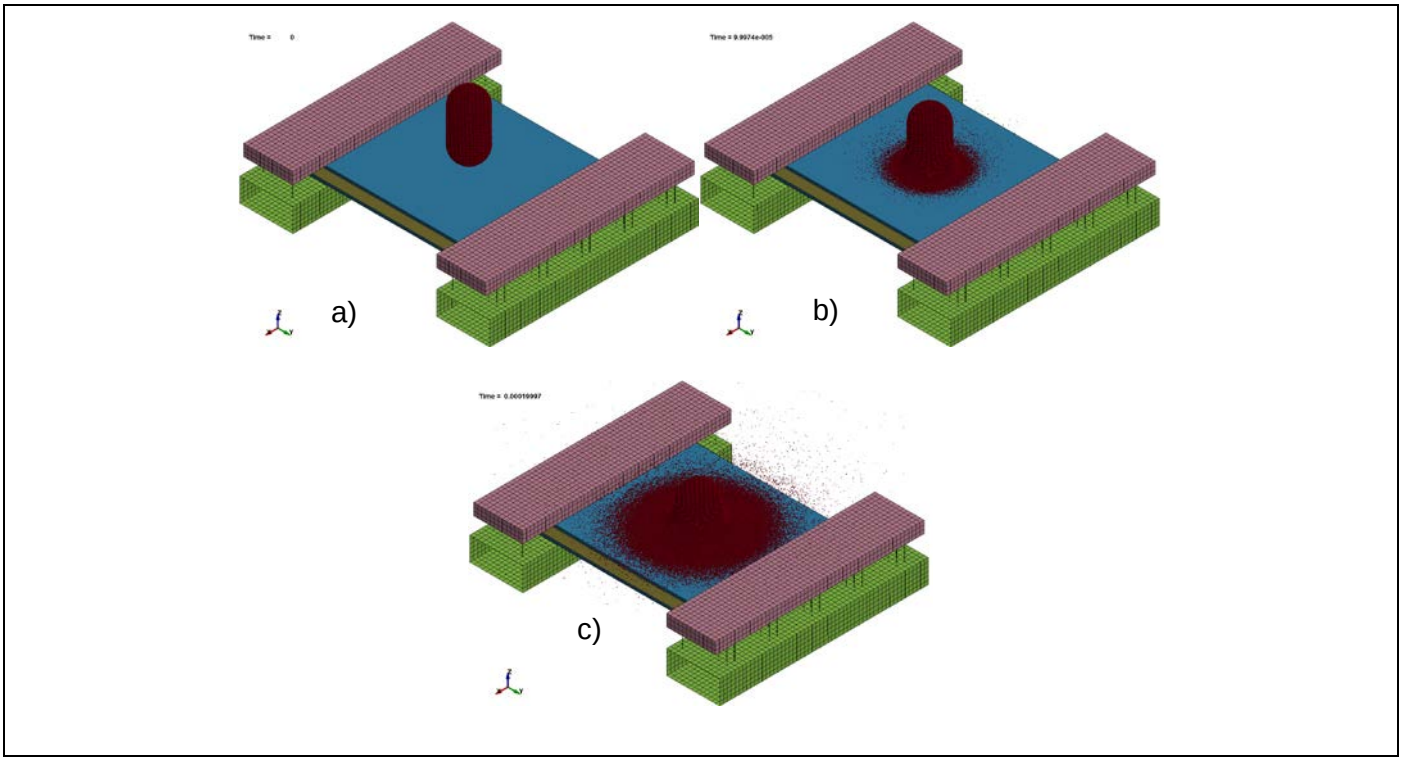

Figure 14: Views of complete model including composite panel, projectile and sample supports during initial stage if impact. Images are for a) t = 0.0 ms, b) t = 0.1 ms, c) t=0.2 ms for impact velocity V_{dt} = 115 m/s.

4.3 Analysis of results

As already stated, the objective of the research was to investigates soft body impact performance of composite sandwich panels with corrugated and tubular core reinforcements. This type of panel with augmented strength and stiffness in one direction is of high importance for specific aerospace applications. The panels were subjected to high velocity impact with soft gelatine projectile as used in bird strike tests. Ideally these panels should have high impact resistance, i.e. suffer minimal damage in impact events and maintain its original structural characteristics. For these panels energy absorption was not considered as an important performance parameter. These are the main reasons why damage assessment and numerical model validation was performed as presented below.

The numerical analyses presented in this section provide information about transient response of the panels to the impact loading including imitation and evolution of damage and predict the final extent of damage to the panels. The predicted damage is compared with the experimentally observed damage allowing for

validation of the simulation results. Finally, a projectile impact on a conventional sandwich panel of equivalent thickness was modelled using the validated modelling approach. This provided a benchmark against which the impact resistance of the corrugated and tubular sandwich panels can be compared.

To improve visibility and readability of numerical results the region of interest was reduced to neighbourhood of impact location (see Figure 15) and the mesh was hidden. Dimensions of the region of interest, for both corrugated and tubular panels, are 50 x 40 mm with a centre corresponding to the impact location.

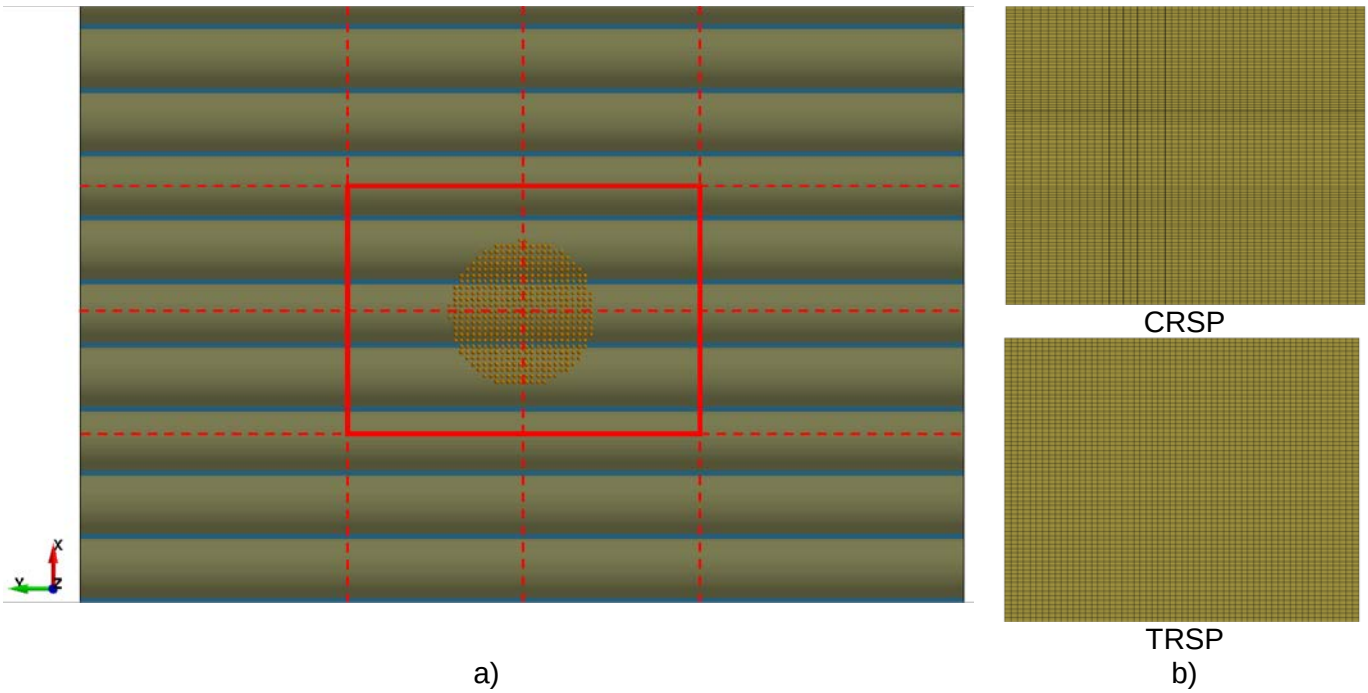

Figure 15 a) Region of interest (red rectangle) for numerical results. b) Detail view of panel mesh for region of interest for both panels.

4.3.1 Corrugated sandwich panel

In the impact tests on CRSP only the impacted face sheets suffered damage primarily due to through thickness tension. The damage distribution was not symmetrical as it can be seen in Figure 16. This was caused by the material anisotropy, architecture of the corrugated reinforcement and the alignment between SPH particles and the irregular finite element mesh of the panel. It is interesting to observe that the areas where the damage extends horizontally from the central damaged area in Figure 16 lay between the corrugation face sheet interfaces. No damage was observed in the corrugated reinforcement nor in the back-face sheet.

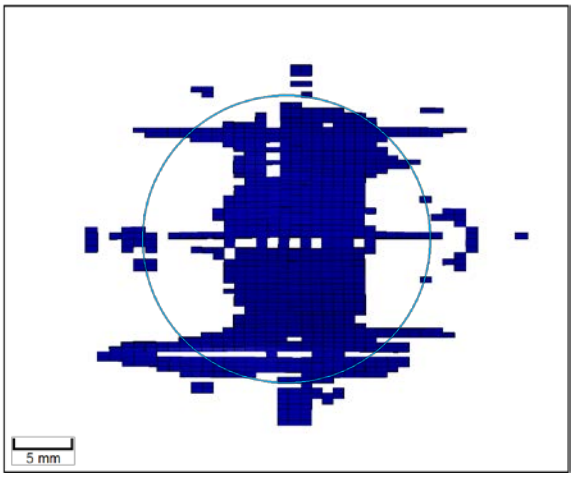

Figure 16: The final damage distribution on the impacted face sheet for the CRSP. Dark blue indicates elements where the through thickness tensile failure criterion was triggered. Light blue circle indicates the original projectile diameter and the impact location.

4.3.2 Sandwich panel with tubular reinforcement

For impact velocity V_i = 115 m/s no damage was predicted for the TRSP composite which agrees with the experimental results. The impacts with the velocity V_i = 235 m/s resulted in significant damage in TRSP. The damage in the impacted face sheet, shown in Figure 17 a), is spread around the impact location. Analysis of the history variables indicate that this damage was caused by through thickness tension. The extent of the damage in the top face sheet is more extensive than shown in the CT images (Figure 10). The damage in the tubes has not been captured, Figure 17 (b).

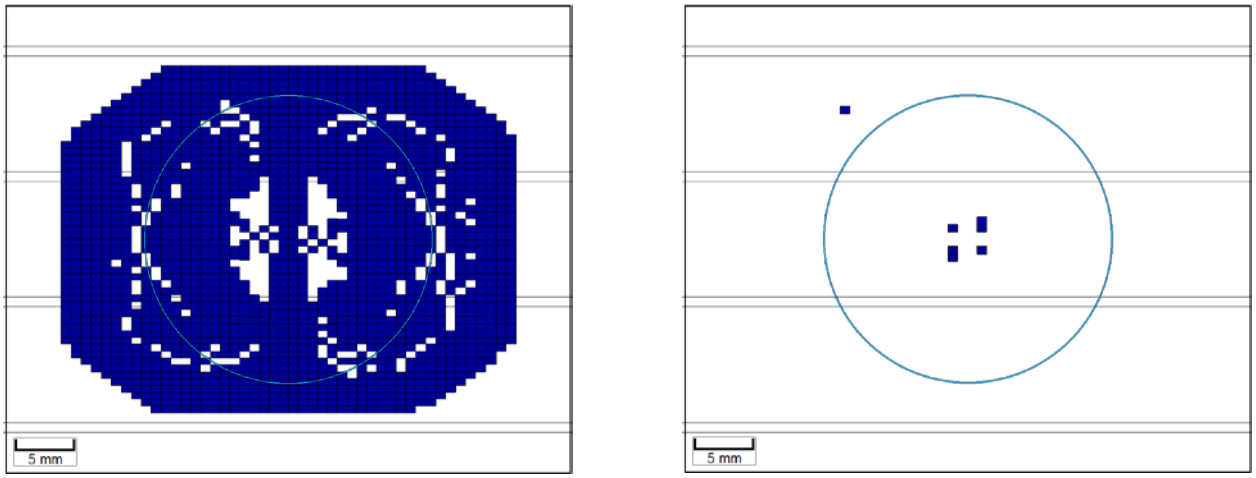

a) b)

Figure 17 Damage distribution for TRSP (a) Impacted face sheet, (b) Tubes. Dark blue indicates elements where the through thickness tension failure criterion was triggered. Light blue circle shows original projectile diameter and location, and the grey lines show the tube locations.

Inaccurate prediction of delamination in the numerical modelling is mainly related to the limitation of the damage criterion incorporated within MAT 59 [62] and differences between the CFRP tube and plate material not represented in the model. Figure 18 below shows failure of the composite tubes for cross sections defined in Figure 10.

4.3.3 Comparison of panel results

To support the use of the simulation results to inform the analysis of the experimental data, a reference panel model (RefSP) was also simulated. The reference panel represents a sandwich panel with only foam between the two face sheets. The model analysed was based on the CRSP model with the material model for the corrugated and adhesive parts replaced by the foam model. The mass of the RefSP panel was 0.142 kg, approximately 80% smaller than the mass of the CRSP panel (0.181 kg). The model of the reference sandwich panel had mass of 0.98 kg.

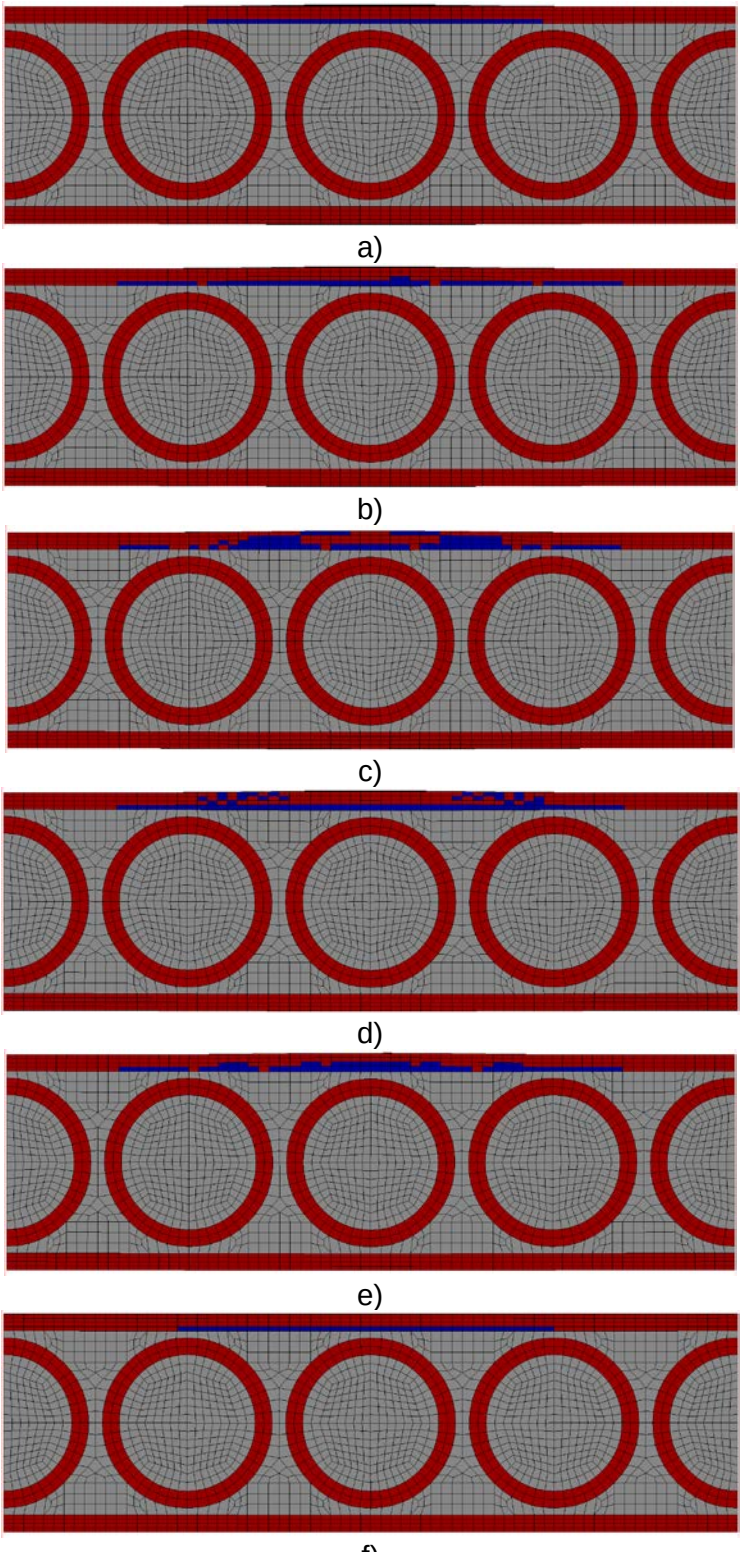

Figure 18: Cross sections of TRSP panel showing extent of failure in the composite section for V_{dt} = 235 m/s. Dark blue indicates elements where the through thickness tension failure criterion was triggered, red elements have not failed. The cross section shown are: a) 63 mm, b) 71 mm, c) 79 mm, d) 85 mm, e) 90 mm, f) 98 mm.

The final deflected shape of each panel simulation is shown in Figure 19. None of the TRSP simulations shows significant deformation at the impact location, while the CRSP model shows local deflection of the impacted sheet and corresponding crushing of the foam. By comparison, the RefSP simulations shows comparatively large local and global deformation, with significant local deformation of the face sheets and foam core at the impact location. This difference in behaviour is also evident from the time-history for the rear surface deflection at the impact point, Figure 20. The peak deflection of the TRSP model for the impact at V_i = 115 m/s is 0.8 mm against 3.9 mm for the CRSP model.

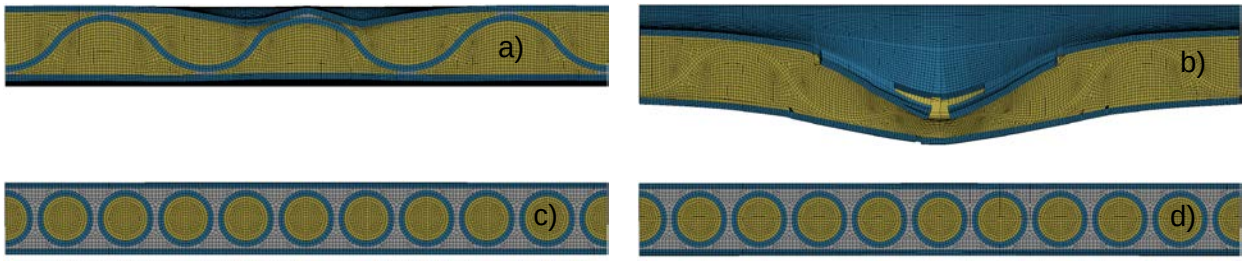

Figure 19: Panel cross-section at the initial impact location at response time t = 2.0 ms. a) CRSP; b) RefSP; c) TRSP at V_{dt} = 115 m/s; d) TRSP at V_{dt} = 235 m/s

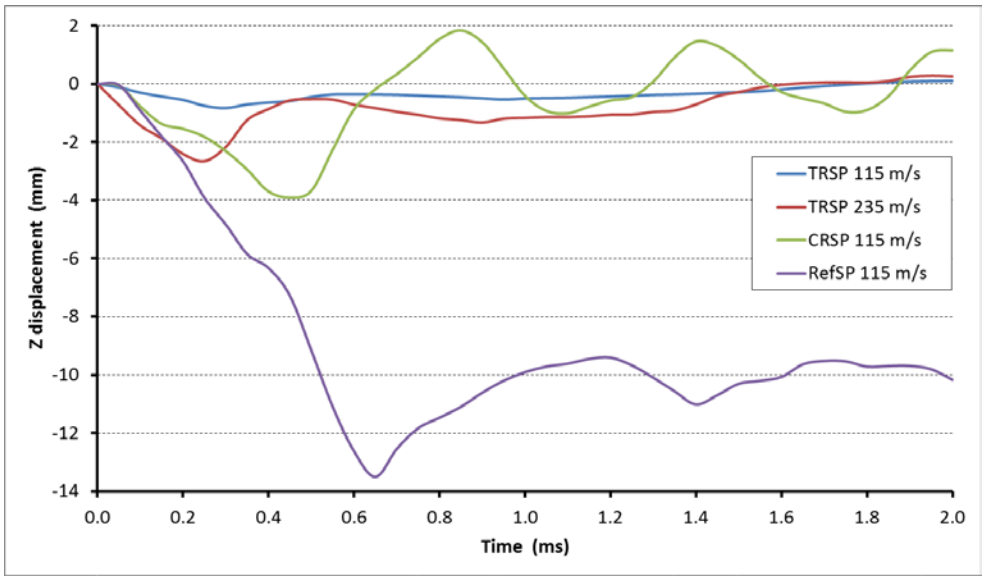

Figure 20: Deflection time history of the centre of the panel rear surface.

The overall bending stiffness of the panels influences the deflection history and to investigate this difference an implicit eigenvalue analysis was performed in LS-DYNA for each model. In order to determine eigenmodes and eigenvalues for the clamped panel, the panel supports were represented by nodal

constraints over the region of the panel in contact with the supports. The resulting eigenfrequency values for the first bending mode for each panel were: 3659 /ms for the TRSP; 1800 /ms for the CRSP; 1621 /ms for the RefSP. These values show that the TRSP panel is significantly stiffer as, despite its greater mass, the natural frequency is significantly higher.

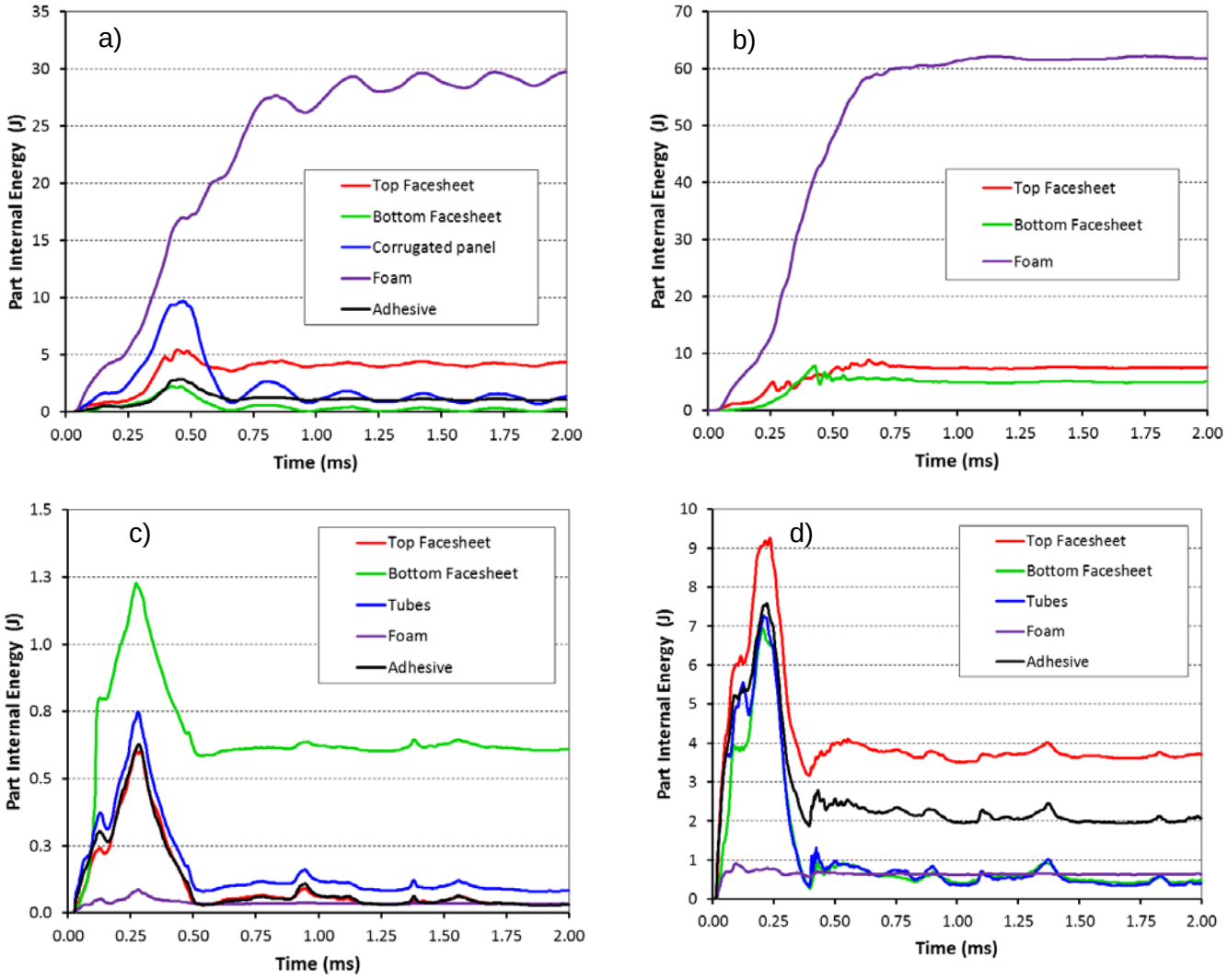

Figure 21: Part internal energy time histories for: a) CRSP; b) RefSP; c) TRSP at V_{dt} = 115 m/s; d) TRSP at V_{dt} = 235 m/s. The scale on the vertical axis is different in each graph.

The part internal energy time-histories, Figure 21, further illustrate the differences between the behaviour observed in the models. The primary mechanism for dissipation in the CRSP model is crushing of the foam core combined with failure in the impacted face sheet. The response of the corrugated insert is primarily elastic as the final part strain energy is lower than the peak value. By comparison the response of the TRSP is primarily elastic, and the energy values measures are small compared to the CRSP model.

5 Conclusions

Impact tests with gelatine projectiles were performed in order to investigate and assess the soft body impact resistance of two the two types of composite sandwich panels with enhanced stiffness and strength in one direction which are of interest for specific aerospace applications. The two reinforcement types considered are a sinusoidal corrugated reinforcement and the composite tube reinforcements.

- The pulsed thermography (PT) inspection showed that corrugated sandwich panels were well manufactured with no hidden delaminations. However, some imperfections related to the uneven distribution of the adhesive and uneven height of the corrugated waves of the corrugated panel were visible on the infrared images. The inspection of tubular samples revealed a number of air bubbles underneath the face sheet panels. The air bubbles were mostly located on the periphery of the samples and therefore did not have a strong influence on the impact resistance of the samples.
- X-ray CT imaging provided detailed state of the damage of the samples, showing that the CRSP sample suffered delamination of the impacted face sheet and cracking of the corrugated reinforcement in the vicinity of the impact location.
- The corrugated panels showed relatively good impact resistance for the soft body impact. Two out of three samples suffered from visible erosion damage of the impacted face sheet close to the impact location with very restricted damage of internal structure and no damage to the rear face sheet.
- The tubular panels showed excellent impact resistance for a velocity of V_i = 115 m/s for which no damage was detected.
- Impact velocity V_{DT} = 235 m/s caused visible damage on the impacted surface as well as extensive subsurface damage of sample TRSP_1. CT imaging of the TRSP_1 indicated that delamination and fibre rupture were predominant failure modes of the composite tube reinforcement. Moreover, TRSP_1 suffered from extensive cracking of the adhesive and delamination of the impacted face sheet. Nevertheless, the impact damage was restricted to three central tubes which were located directly under impact point.

- Numerical analyses of the panels showed agreement with the experimental results in terms of the trends in damage between the three experimental conditions. No failure occurred in the TRSP model at the lower impact velocity. At the higher impact velocity, extensive through thickness failure occurred at the impact location. Through thickness failure occurred in the CRSP model at the lower impact velocity. Investigation of the models confirm that the TRSP panel is significantly stiffer than the CRSP panel and that this influences the panel responses.
- The numerical analysis suggests that both CRSP and TRSP are significantly more damage resistant than conventional sandwich panel benchmarks (RefSP). Projectile impact on RefSP resulted in severe damage of the sample, including failure of the top face sheet and significant damage to the foam core.

To conclude the results of the numerical and experimental investigation demonstrate the potential of reinforced core sandwich panels in terms of soft body (bird strike) impact resistance at speeds representative of take-off or and landing scenarios. Additional studies are required to investigate a number of avenues. Firstly, to ascertain experimentally and through modelling the sensitivity to impact at different locations with respect to the reinforcements, to optimise the reinforcement morphology and design to further increase impact resistance, and to assess the effect of soft body impact with larger projectiles are required to assess the performance of the samples for higher impact energies. Finally, studies need to be undertaken to examine the impact resistance of the corrugated and tubular sandwich panels subjected to an impact with a hard impactor.

Acknowledgements

We acknowledge the University of Manchester for providing the financial support for this research. The Manchester Henry Moseley X-ray Imaging Facility was funded in part by the EPSRC (grants EP/F007906/1, EP/F001452/1 and EP/I02249X/1) and the HEFCE grant for the Multidisciplinary Characterisation Facility.

References

[1] Hazizan, M. A. & Cantwell, W. J., 2002. The low velocity impact response of foam-based sandwich structures. Composites Part B: Engineering, 33(3), pp. 193-204.

[2] DVA, 2009. Boeing 747-400 Aircraft Operations Manual.

[3] France A., 2010. Airbus A380-800.

[4] Raju, K. S. et al., 2008. Impact damage resistance and tolerance of honeycomb core sandwich panels. Journal of Composite Materials, 42(4), pp. 385-412.

[5] Abrate, S., 1997. Localised impact on sandwich structures with laminated facings. Applied Mechanics Reviews, 50(2), pp. 69-82.

[6] Baral, N. et al., 2010. Improved impact performance of marine sandwich panels using through-thickness reinforcement: Experimental results. Composites Part B: Engineering, 41(2), pp. 117-123.

[7] Gustin J., Joneson A., Mahinfalah M. & Stone, J., 2005. Low velocity impact of combination Kevlar/carbon fibre sandwich composites. Composite Structures, 69(4), pp. 396-406.

[8] Horrigan, D. P. W., Aitken, R. R. & Moltschaniwskyj, G., 2000. Modelling of crushing due to impact in honeycomb sandwiches. Journal of Sandwich Structures and Materials, 2(2), pp. 131-151.

[9] Wada A., Kawasaki T., Minoda Y., Kataoka A., Tashiro S., Fukuda H., 2003, A method to measure shearing modulus of the foamed core for sandwich plates, Compos. Struct. 60, pp. 385–390.

[10] Charles, J.-P. & Guedra-Degeorges, D., 1991. Impact damage tolerance of helicopter sandwich structures. Advanced Materials/Affordable Processes., Volume 23, pp. 51-61.

[11] Mines, R. A. W., Worrall, C. M. & Gibson, A. G., 1998. Low velocity perforation behaviour of polymer composite sandwich panels. International Journal of Impact Engineering, 21(10), pp. 855-879.

[12] Heimbs S., Schmeer S., Middendorf P., Maier M., 2007. Strain rate effects in phenolic composites and phenolic-impregnated honeycomb structures. Compos Sci Technol., 67, pp. 2827–37.

[13] Mahfuz, H., Al Mamum, W. & Jeelani, S., 1992. Effect of core density and implanted delamination on the high strain rate response of foam core sandwich composites. Sandwich Constructions, Volume 5, pp. 597-606.

[14] Rhodes, M. D., 1975. Impact fracture of composite sandwich structures. Denver, AIAA.

[15] Flores-Johnson, E. A. & Li, Q. M., 2011. Experimental study of the indentation of sandwich panels with carbon fibre-reinforced polymer face sheets and polymeric foam core. Composites Part B: Engineering, 42(5), pp. 1212-1219.

[16] Wang, J., Waas., A. M. & Wang, H., 2013. Experimental study on the low-velocity impact behaviour of foam-core sandwich panels. Composite structures, February, pp. 298-311.

[17] Torre, L. & Kenny, J. M., 2000. Impact testing and simulation of composite sandwich structures for civil transportation. Composite Structures, 50(3), pp. 257-267.

[18] Vaidya, U. K., Nelson, S., Sinn, B. & Mathew, B., 2001. Processing and high strain rate impact response of multi-functional sandwich composites. Composite Structures, Volume 52, pp. 429-440.

[19] Lascoup, B., Aboura, Z., Khellil, K. & Benzeggagh, M., 2010. Impact response of three-dimensional stitched sandwich composite. Composite Structures, 92(2), pp. 347-353.

[20] Vaidya, A. S., Vaidya, U. K. & Uddin, N., 2008. Impact response of three-dimensional multifunctional sandwich composite. Materials Science and Engineering: A, Volume 472, pp. 52-58.

[21] Arias A., Zaera R., Lopez-Puente J., Navarro C., 2003, Numerical modelling of the impact behaviour of new particulate loaded composite materials, Compos. Struct. 61, pp. 151–159.

[22] Shim V.P.W., Yap K.Y., 1997, Modelling impact deformation of foam-plate sandwich systems, Int. J. Impact Eng. 19, pp. 615–636.

[23] Hou S.J., Ren L.L., Dong D., Han X., 2012, Crashworthiness optimization design of honeycomb sandwich panel based on factor screening. J Sandwich Struct Mater, 14(6), pp. 655–78.

[24] Hou S.J., Shu C.F., Zhao S.Y., Liu T.Y., Han X., Li Q., 2015, Experimental and numerical studies on multi-layered corrugated sandwich panels under crushing loading. Compos Struct, 126, pp. 371–85.

[25] Lopatnikov S.L., Gama B.A., Haque M.J., Krauthauser C., Gillespie J.W., Guden M., Hall I.W., 2003, Dynamics of metal foam deformation during Taylor cylinder–Hopkinson bar impact experiment, Compos. Struct. 61, pp. 61–71.

[26] Abrate S., 1998, Impact on Composite Structures, Cambridge University Press, Cambridge,

[27] Mohmmed, R., Zhang, F., Sun, B. & Gu, B., 2013. Finite element analyses of low-velocity impact damage of foam sandwiched composites with different ply angles face sheets. Materials \& Design, 47(0), pp. 189-199.

[28] Shi Y., Swait T., Soutis C., 2012, Modelling damage evolution in composite laminates subjected to low velocity impact. Compos Struct, 94, pp. 2902–13.

[29] Tanoglu M., Seyhan A.T., 2002, Investigating the effects of a polyester performing binder on the mechanical and ballistic performance of E-glass fibre reinforced polyester composites, Int. J. Adhes. Adhes. 23, pp. 1–8.

[30] Aktay L., Johnson A.F., Holzapfel M., 2005, Prediction of impact damage on sandwich composite panels. Comput. Mater. Sci., 32(3), pp. 252-60.

[31] Elmarakbi, A. M., Hu, N. & Fukunaga, H., 2009. Finite element simulation of delamination growth in composite materials using LS-DYNA. Composites Science and Technology, 69(14), pp. 2383-2391.

[32] Feng D., Aymerich F., 2013, Damage prediction in composite sandwich panels subjected to low-velocity impact. Compos Part A Appl Sci Manuf, 52, pp. 12-22.

[33] Foo C.C., Chai G.B., Seah L.K., 2008, A model to predict low-velocity impact response and damage in sandwich composites. Compos Sci Technol.; 68: pp. 1348–56.

[34] Zhou J., Hassan M.Z., Guan Z., Cantwell W.J., 2012, The low velocity impact response of foam-based sandwich panels. Compos Sci Technol, 72(14), pp. 1781-90.

[35] Kilchert S., Johnson A.F., Voggenreiter H., 2014, Modelling the impact behaviour of sandwich structures with folded composite cores. Compos Part A Appl Sci Manuf, 57, pp. 16–26.

[36] Menna C., Manes Z.A., Asprone D., Prota A., 2013, Numerical assessment of the impact behaviour of honeycomb sandwich structures. Compos Struct, 106, pp. 326–39.

[37] Schwab M., Todt M., Wolfahrt M., Pettermann H.E., 2016, Failure mechanism-based modelling of impact on fabric reinforced composite laminates based on shell elements. Compos Sci Technol., 128, pp. 131–7.

[38] Sokolinsky V.S., Indermuehle K.C., Hurtado J.A., 2011, Numerical simulation of the crushing process of a corrugated composite plate. Compos Part A Appl Sci Manuf, 42, pp. 1119–26.

[39] Morada G., Ouadday R., Vadean A., Boukhili R., 2017, Low-velocity impact resistance of ATH/epoxy core sandwich composite panels: Experimental and numerical analyses, Composites Part B, 114, pp. 418-431

[40] Besant T, Davies G.A.O., Hitchings D., 2001, Finite element modelling of low velocity impact of composite sandwich panels. Compos Part A, Appl. Sci. Manuf. 32, pp. 1189–96.

[41] UMECO, 2015. Advanced Composites Group Umeco Composites. [Online] Available at: http://html.investis.com/u/umeco/ [Accessed 23 March 2015].

[42] EasyComposites Ltd., 2010. EasyComposites. [Online] Available at: http://www.easycomposites.co.uk/#!/cured-carbon-fibre-products/rigid-carbon-fibre-sheet/Prepreg-Carbon-Fibre-Flat-Sheet.html [Accessed 18 April 2017].

[43] CFS Fibreglass. CFS Fibreglass Supplies. Available online at: http://www.cfsnet.co.uk/acatalog/2_Part_Expanding_Foam_TDS.pdf

[44] Hamershock D.M., Seamans T.W. and Bernhardt G.E., 1993, Determination of Body Density for Twelve Bird Species, WL-TR-93-3049, Wright Laboratory

[45] Lavoie, M. A., 2008. Soft body impact modelling and development of a suitable meshless approach. PhD Thesis.

[46] Lavoie, M. et al., 2009. Bird's substitute tests results and evaluation of available numerical methods. International Journal of Impact Engineering, Volume 36, pp. 1276-1287.

[47] Wilbeck, J. S., 1978. Impact Behaviour of Low Strength Projectiles. Air Force Materials Lab, AFML-TR-77-134.

[48] Seidl, M., Hughes, K. & De Vuyst, T., 2013. Modelling internal gas flows in a single stage gas gun using Eulerian/Lagrangian coupling in LS-DYNA. Manchester, 9th European LS-DYNA users conference.

[49] Budgey, R., 2000. The development of a substitute artificial bird by the international bird strike research group for use in aircraft component testing. International Bird Strike Committee, Report, IBSC25-WP-IE3.

[50] Dolber, R., Wright, S., Weller, J. & Begier, M., 2014. Wildlife strikes to civil aircraft in the United States, 1990 - 2013, Washington: Federal Aviation Administration.

[51] Shepard, S. M., 1997. Introduction to active thermography for non-destructive evaluation. Anti-Corrosion Methods and Materials, 44(4), pp. 236-239.

[52] Shepard, S. M., 2007. Flash thermography of aerospace composites. Buenos Aires, IV Conferencia Panamericana the END.

[53] Widjanarko, T., Tinsley, L., Roy, R., and Mehnen, J., 2012, Characterisation and performance assessment of a pulsed-thermography camera system for component degradation inspection. In 1st International Conference on Through-life Engineering Services Cranfield

[54] Vignjevic, R., Orlowski, M., DeVuyst, T. & Campbell, J. C., 2013. A parametric study of bird strike on engine blades. International Journal of Impact Engineering, Volume 60, pp. 44-57.

[55] McCarthy, M. A. et al., 2005. Modelling bird impacts on an aircraft wing Part 2: modelling the impact with an SPH bird model. Applied Composite Materials, 11(5), pp. 317-340.

[56] Jenq, S. et al., 2007. Simulation of a rigid plate hit by a cylindrical hemi-spherical tip-ended soft impactor. Computational Materials Science, 39(3), pp. 518-526.

[57] Cheng, W. & Hallquist, J., 2004. Implementation of three-dimensional composite failure model into DYNA3D.

[58] LSTC, 2014. LS-DYNA Keyword User's Manual - Volume II (Material Models). R7.1 ed. Livermore, California: Livermore Software Technology Corporation.

[59] Reyes, A. et al., 2003. Constitutive modelling of aluminium foam including fracture and statistical variation of density. European Journal of Mechanics - A/Solids, 22(6), pp. 815-835.

[60] Deshpande, V. S. & Fleck, N. A., 2000. Isotropic constitutive models for metallic foams. Mechanics and Physics of Solids, Volume 48, pp. 1253-1283.

[61] Reyes, A., Hopperstad, O. S., Berstad, T. & and Langseth, M., 2004. Implementation of a constitutive model for aluminium foam including fracture and statistical variation of density. Dearborn, Michigan, 8th LS-DYNA user conference.

[62] LSTC, 2014. MAT59 solid s.l.:http://ftp.lstc.com/anonymous/outgoing/jday/composites/mat59_solids.

[63] Michael Orlowski, Experimental and Numerical Investigation on the Bird Impact Resistance of Novel Composite Sandwich Panels, PhD thesis, Cranfield University